nature immunology

Article

https://doi.org/10.1038/s41590-025-02359-5

Lymphotoxin-dependent elevated meningeal CXCL13:BAFF ratios drive gray matter injury

Received: 7 January 2025

Accepted: 4 November 2025

Published online: 2 January 2026

Check for updates

Ikbel Naouar[1], Andrei Pangan[1], Michelle Zuo[1], Syed Ali Raza[2], Kevin Champagne-Jorgensen[1], Jyot Patel[1], Angela Wang[1], Annie Pu[1], Lesley Ward[1], Jennifer S. Y. Ahn[1], Faizah N. Sayeed[1], Jingwen Zhu[1], Elisabeth Pössnecker[3,4,5,6,7], Shoshana Spring[8], John G. Sled[8], Bruno Cenni[9], Barbara Nuesslein-Hildesheim[9], Jeffrey L. Browning[10], Anne-Katrin Pröbstel[3,4,5,6,7], Daniel S. Reich[2], Jennifer L. Gommerman[1] ✉ & Valeria Ramaglia[1,11] ✉

In multiple sclerosis (MS), B cell-rich tertiary lymphoid tissues (TLTs) in the brain leptomeninges associate with cortical gray matter injury. Using a model of Th17 cell-driven experimental autoimmune encephalomyelitis in mice, we found that inhibitors of Bruton's tyrosine kinase (BTKi) prevented TLT formation and cortical pathology in a B cell activating factor (BAFF)-dependent manner. BTKi reduced expression of lymphotoxin ligands, and cotreatment with a lymphotoxin-β receptor agonist abrogated the benefits of BTKi. TLT and cortical pathology tracked with a high CXCL13:BAFF ratio in the leptomeninges, which was reduced by BTKi. Moreover, we observed high CXCL13:BAFF ratios in post mortem cerebral spinal fluid from patients with MS and pathologically confirmed leptomeningeal inflammation, as well as in living patients with MS and radiologically confirmed paramagnetic rim lesions. In summary, using experimental autoimmune encephalomyelitis, we revealed a molecular circuit that leads to TLT formation and cortical injury with translational relevance for detection of this pathology in patients with MS.

The frequent observation of lymph node-like organized aggregates of immune cells in chronically inflamed tissues[1], which we refer to as tertiary lymphoid tissues (TLTs)[2], suggests that lymphoid tissue neogenesis may have a role in supporting immune responses at sites of chronic inflammation. Pathological studies of brains from people with multiple sclerosis (MS) have demonstrated the formation of TLTs of variable sizes and organization in the brain leptomeninges of the central nervous system (CNS)[3–9]. These TLTs are rich in B cells[3] and are associated with underlying gray matter injury including (subpial pattern) cortical demyelination, neuronal loss, microglial activation and a more severe disease course[5,6,8,10].

The mechanistic steps that lead to leptomeningeal TLT are unknown. Moreover, fluid biomarkers or radiological proxies of TLT and gray matter injury are lacking[11,12]. Current MS therapies are effective at reducing white matter lesions[13], which can be easily tracked radiologically. However, (cortical) gray matter lesions have a different and ill-understood etiology[14], with no effective treatment. Gray matter lesions ultimately lead to neurodegeneration and brain volume loss in MS[15].

Rodent models of MS (experimental autoimmune encephalomyelitis, EAE) that recapitulate brain leptomeningeal TLTs[2,16] represent our best tool for studying the molecular requirements for TLT

A full list of affiliations appears at the end of the paper. ✉e-mail: jen.gommerman@utoronto.ca; valeria.ramaglia@uhn.ca

formation. We previously described a passive model of EAE whereby myelin-primed Th17 cells adoptively transferred into SJL/J recipient mice induce paralysis and robust leptomeningeal TLTs[2]. Compared to young SJL/J recipient mice, old SJL/J recipients exhibit severe and unremitting axon and synapse loss accompanied by brain atrophy[17]. In both aged and young recipients, TLTs are associated with degradation of the glial limitans and an inward gradient of subpial cortical demyelination and microglia/macrophage accumulation[2,18], as seen in MS[5,6,8].

Remibrutinib (LOU064) is a brain-penetrant selective covalent inhibitor of Bruton's tyrosine kinase (BTKi)[19] and has shown pharmacologic efficacy in rodent models of MS but has not been tested for its impact on cortical pathology[20–23]. Herein, we used remibrutinib to define the circuitry that drives leptomeningeal TLT and used these findings to identify a potential biofluid-based means for ascertaining brain-compartmentalized inflammation in MS.

Results

BTK inhibition prevents subpial injury in young EAE

Bruton's tyrosine kinase (BTK) is an intracellular kinase that mediates signals initiated by surface receptor engagement emanating from the B cell receptor on B cells and the FcγR on myeloid cells[20]. Given the therapeutic efficacy of B cell depletion in MS[13], BTK has been tested as a therapeutic target[24]. To determine the impact of BTKi on subpial cortical gray matter pathology independent of its role in T cell priming, we adoptively transferred myelin-specific Th17 cells primed in untreated SJL/J donor mice into recipient mice to induce EAE. EAE mice were then prophylactically treated with BTKi before the onset of clinical symptoms until endpoint (Extended Data Fig. 1a). This treatment regimen resulted in a significant accumulation of the drug in the spleen (Extended Data Fig. 1b) and in the brain (Extended Data Fig. 1c). Pre-primed myelin-specific Th17 cells drive spinal cord white matter injury and paralysis in EAE[25,26], and enter the leptomeninges before B cell accumulation at this site. Thus, similar to what we have previously observed in mice treated with a B cell depleting agent (anti-CD20)[27], BTK inhibition did not significantly impact spinal cord-related readouts, including paralysis (Extended Data Fig. 1d–g), the accumulation of neurofilament light (NfL) chain in the serum (Extended Data Fig. 1h,i) or spinal cord pathology (Extended Data Fig. 2).

We previously showed that the cortex, including the glial limitans, is injured in areas adjacent to the TLT but not in areas distal to the TLT[18]. Therefore, we next examined the impact of BTKi on cortical demyelination and microgliosis, both of which are associated with disease progression in MS[4,5,8]. Immunohistochemistry of subpial cortical gray matter showed that, compared to vehicle-treated controls, treatment with BTKi reduced disruption of the glial limitans, cortical demyelination, myeloid cell accumulation and axonal loss (Fig. 1a–d). Importantly, in addition to prophylactic administration, the protective effects of BTKi in the cortex were also observed in a therapeutic drug delivery modality (Fig. 1 and Extended Data Fig. 3). In summary, BTKi abrogates cortical pathology in a passive model of EAE.

BTK inhibition prevents subpial injury in old EAE

Brain atrophy is a key feature of aged MS[28,29] and in the aged version of our EAE model[17]. Therefore, we assessed whether BTKi protects the brain from atrophy and subpial cortical gray matter pathology in old mice that received pre-primed Th17 cells (Extended Data Fig. 4). As in young mice, BTK inhibition did not impact paralysis as expected (Extended Data Fig. 4). Using 7-tesla magnetic resonance imaging (7T MRI) we assessed the impact of BTKi on brain volume. Excitingly, therapeutic administration of BTKi ameliorated whole brain atrophy, with beneficial effects particularly observed in the somatosensory cortex (SSC) (Fig. 2a). Moreover, compared to vehicle-treated controls, mice treated with BTKi exhibited reduced disruption of the glial limitans, minimal cortical demyelination and myeloid cell accumulation, as well as reduced axonal injury (Fig. 2b–e). In summary, therapeutic administration of BTKi abrogates brain atrophy and cortical pathology in aged EAE mice.

Enforced LTβR signaling overrides BTKi neuroprotection

We next asked whether the protection conferred by BTKi on brain pathology is connected with leptomeningeal TLT formation. We found that, compared to vehicle-treated controls, BTKi reduced both the number and size of TLTs adjacent to the cortex (Fig. 3a,b) and generally throughout the brain meninges (Extended Data Fig. 5). In vehicle-treated controls, TLTs were largely populated by $B220^+$ B cells and $CD3^+$ T cells—both cell populations were significantly reduced in BTKi-treated mice, with remaining B cells appearing dispersed through the leptomeninges (Fig. 3c and Extended Data Fig. 6). While we did not phenotype BTKi-sensitive B cells in the leptomeninges, we previously showed that not only mature but also anti-CD20 resistant immature B cells accumulate in the leptomeninges during EAE[30]. Future work should address which of these B cell subsets respond to BTKi.

We previously showed that accumulation and organization of B cells in the inflamed leptomeninges is mediated by lymphotoxin-β receptor (LTβR)-derived signals in radioresistant stromal cells[2]. Lymphotoxin (LT)α and LTβ form a membrane-bound heterotrimer (LTα1β2) that stimulates LTβR, which is primarily expressed by stromal cells and myeloid cells. LTβR signaling in fibroblasts is required for lymph node development in utero and can promote TLT in various tissues[31]. Given that TLTs were blunted in BTKi-treated EAE mice, we hypothesized that BTKi may be indirectly impacting LTβR signaling in stromal cells by interfering with the expression of LTβR ligands in a BTK-sensitive target cell. Strengthening this hypothesis, using quantitative PCR (qPCR) we observed a significant reduction in *Ltb* and a nonsignificant trend in reduced *LTa* expression in the leptomeninges of BTKi-treated EAE (Fig. 4a).

We therefore assessed the expression of *Btk*, *Lta* and *Ltb* in the inflamed leptomeninges by mining our previously published single-cell RNA sequencing (scRNAseq) database of leptomeninges from young versus old EAE mice at the acute timepoint[17]. We found that the expression of *Btk*, *Lta* and *Ltb* in the leptomeningers was comparable between young and old EAE mice, and that *Btk* expression was primarily observed in leptomeningeal B cells and, to a lesser extent, in myeloid cells. *Ltb* was expressed in B and T cells as well as neutrophils and $Ly6c^+$ myeloid cells. In general, *Lta* expression was less pronounced than *Ltb* (Fig. 4b) in line with previous data reporting that *Lta* expression is regulated differently than *Ltb*, and potentially less stable[32]. Importantly, *LTa*, *Ltb* and *Btk* were found to be co-expressed only in B cells (Fig. 4c,d).

Given the unique expression of LT ligands and *Btk* in B cells in the inflamed leptomeninges, we next performed an in vitro experiment where we pretreated naive SJL/J splenocytes with BTKi, then stimulated splenocytes with anti-CD40 and lipopolysaccharide (LPS). This in vitro protocol significantly induced the upregulation of LTαβ surface protein detected by LTβR-Ig flow cytometry compared to $Ltb^{-/-}$ splenocytes (Extended Data Fig. 7). Compared to vehicle treated splenocytes, we found a lower percentage of $LT\alpha\beta^+$ B cells among stimulated splenocytes treated with BTKi (Fig. 4e). In summary, B cells uniquely express *Lta*, *Ltb* and *Btk* in inflamed leptomeninges, and the upregulation of LTαβ on activated B cells is BTK-dependent.

To determine if LTβR signaling was causally associated with BTK-driven subpial cortical gray matter damage and microgliosis in EAE mice, we administered an LTβR agonist antibody (αLTβR)[33] at days 9 and 11 post-adoptive transfer of Th17 cells, concomitant with BTKi treatment. Combined BTK inhibition and αLTβR treatment reversed the beneficial effects conferred by BTKi alone on disruption of the glial limitans, demyelination, microgliosis and axonal loss in the subpial gray matter (Fig. 5a–d). In summary, these data link BTK with LTβR-mediated signals in mediating subpial gray matter damage.

https://doi.org/10.1038/s41590-025-02359-5

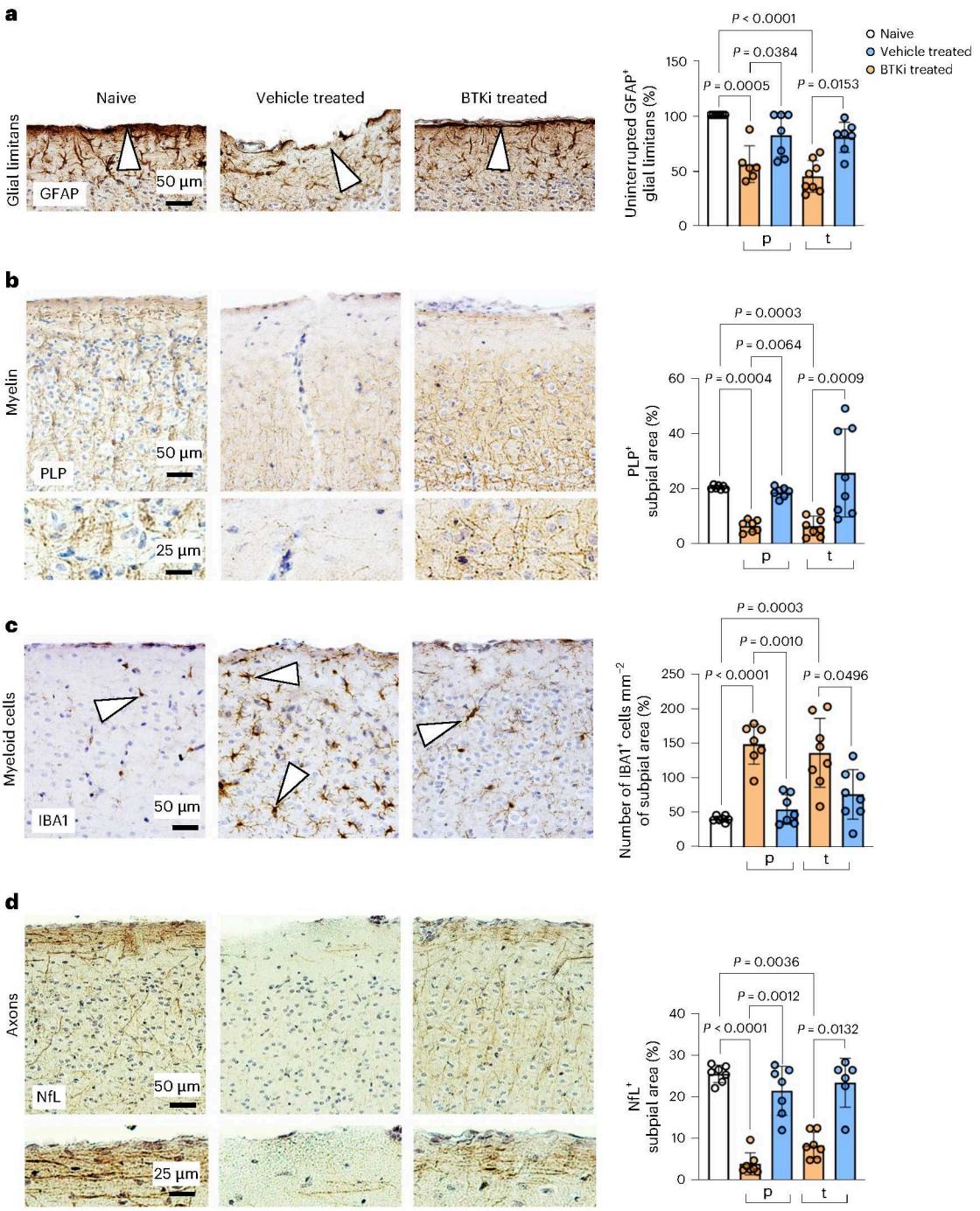

Fig. 1 | BTK inhibition spares the glial limitans and prevents cortical gray matter demyelination, myeloid cell accumulation and axonal loss in young SJL/J adoptive transfer EAE mice. a–**d**, Immunohistochemical staining and quantification of SSC tissue from naive, vehicle-treated and BTKi-treated SJL/J adoptive transfer EAE mice at peak disease (day 12 after adoptive transfer) for GFAP visualizing the glial limitans (**a**) (naive $n = 7$, p-vehicle treated $n = 6$, p-BTKi treated $n = 7$, t-vehicle treated $n = 8$ and t-BTKi $n = 7$), proteolipid protein (PLP) visualizing myelin (**b**) (naive $n = 7$, p-vehicle treated $n = 7$, p-BTKi treated $n = 7$, t-vehicle treated $n = 8$ and t-BTKi $n = 7$), ionized calcium binding adapter molecule 1 (IBA1) visualizing microglia and macrophages (**c**) (naive $n = 7$, p-vehicle treated $n = 7$, p-BTKi treated $n = 7$, t-vehicle treated $n = 8$ and t-BTKi $n = 8$), and NfL visualizing axons (**d**) (naive $n = 7$, p-vehicle treated $n = 7$, p-BTKi treated $n = 7$, t-vehicle treated $n = 7$ and t-BTKi $n = 6$). White arrowheads in **a** indicate the glial limitans; those in **c** indicate microglia/macrophages. Zoomed subpial areas are taken at equivalent depth from the pia mater across groups. Data are shown as mean ± s.d. Statistical analysis was conducted using Kruskal–Wallis tests. p, prophylactic; t, therapeutic.

BTKi alters leptomeningeal CXCL13 and BAFF

Passive transfer of encephalitogenic Th17 cells into SJL/J mice results in an approximately 800-fold increase in *Cxcl13* that is exquisitely LTβR-dependent[2]. Given that BTKi reduced the expression of LTβR ligands in the leptomeninges, we next wished to determine if BTKi inhibition affects CXCL13 accumulation in this compartment. Staining for CXCL13 protein within TLT revealed significantly reduced leptomeningeal CXCL13 staining in BTKi-treated mice compared to control-treated mice. In contrast, the combination of BTKi with LTβR agonism reversed the CXCL13 reduction induced by BTKi treatment alone (Fig. 6a).

https://doi.org/10.1038/s41590-025-02359-5

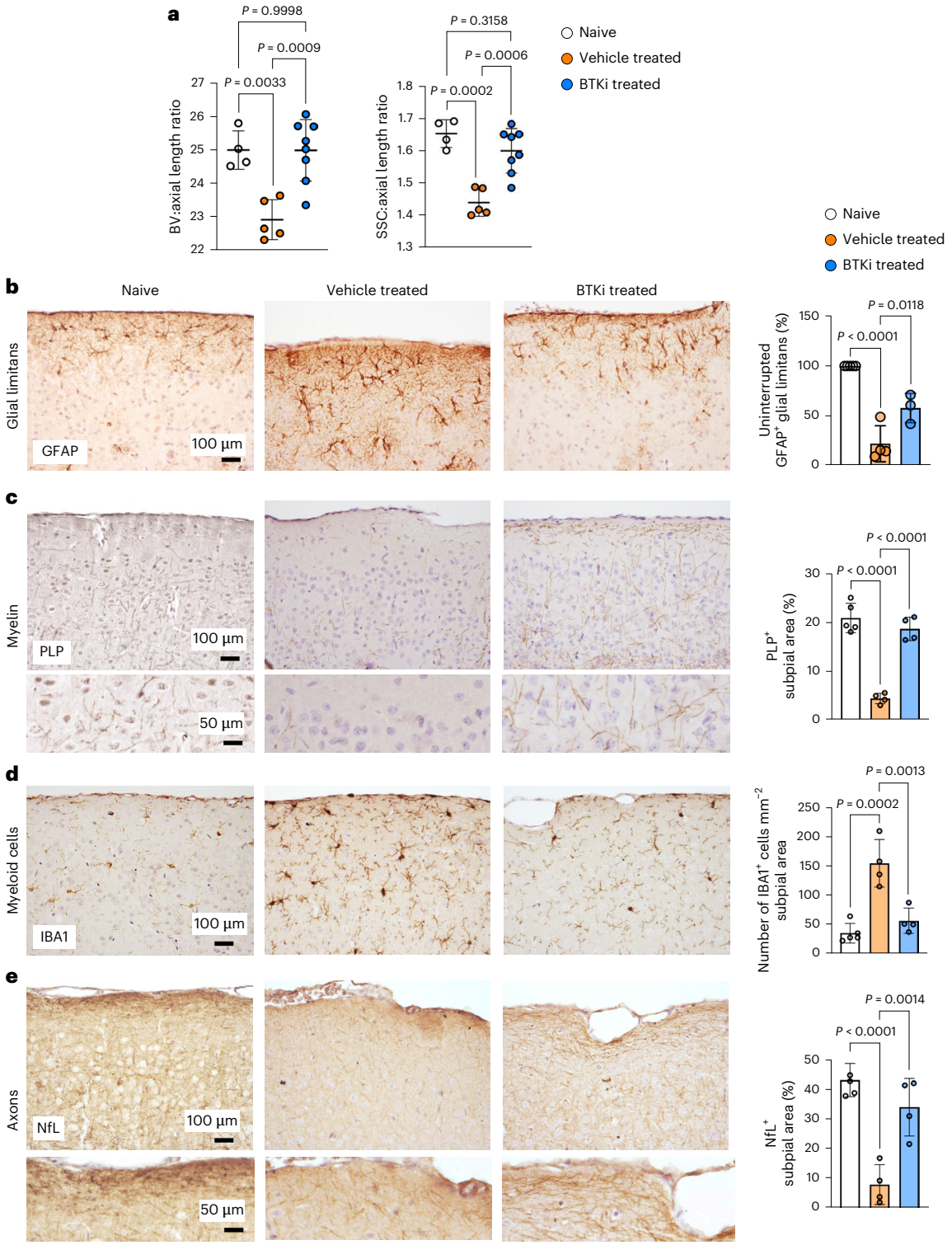

Fig. 2 | BTK inhibition prevents brain atrophy, spares the glial limitans and prevents cortical gray matter demyelination, myeloid cell accumulation and axonal loss in old SJL/J adoptive transfer EAE mice. a, Post mortem 7T MRI findings of whole brain volume (BV) and volume of the SSC from naive ($n = 4$), EAE vehicle-treated ($n = 5$) and EAE BTKi-treated ($n = 8$) old SJL/J mice, expressed as a ratio to axial length. **b**–**e**, Immunohistochemical staining and quantification of SSC tissue from naive, vehicle-treated and BTKi-treated SJL/J adoptive transfer EAE mice at peak disease (day 12 after adoptive transfer) for GFAP visualizing the glial limitans (**b**), PLP visualizing myelin (**c**), IBA1 visualizing microglia and macrophages (**d**), and NfL visualizing axons (**e**). Zoomed subpial areas are taken at equivalent depth from the pia mater across groups. Naive ($n = 5$), vehicle treated ($n = 4$) and BTKi treated ($n = 4$). Data are shown as mean ± s.d. Statistical analysis was conducted using one-way analysis of variance (ANOVA) with multiple comparison.

https://doi.org/10.1038/s41590-025-02359-5

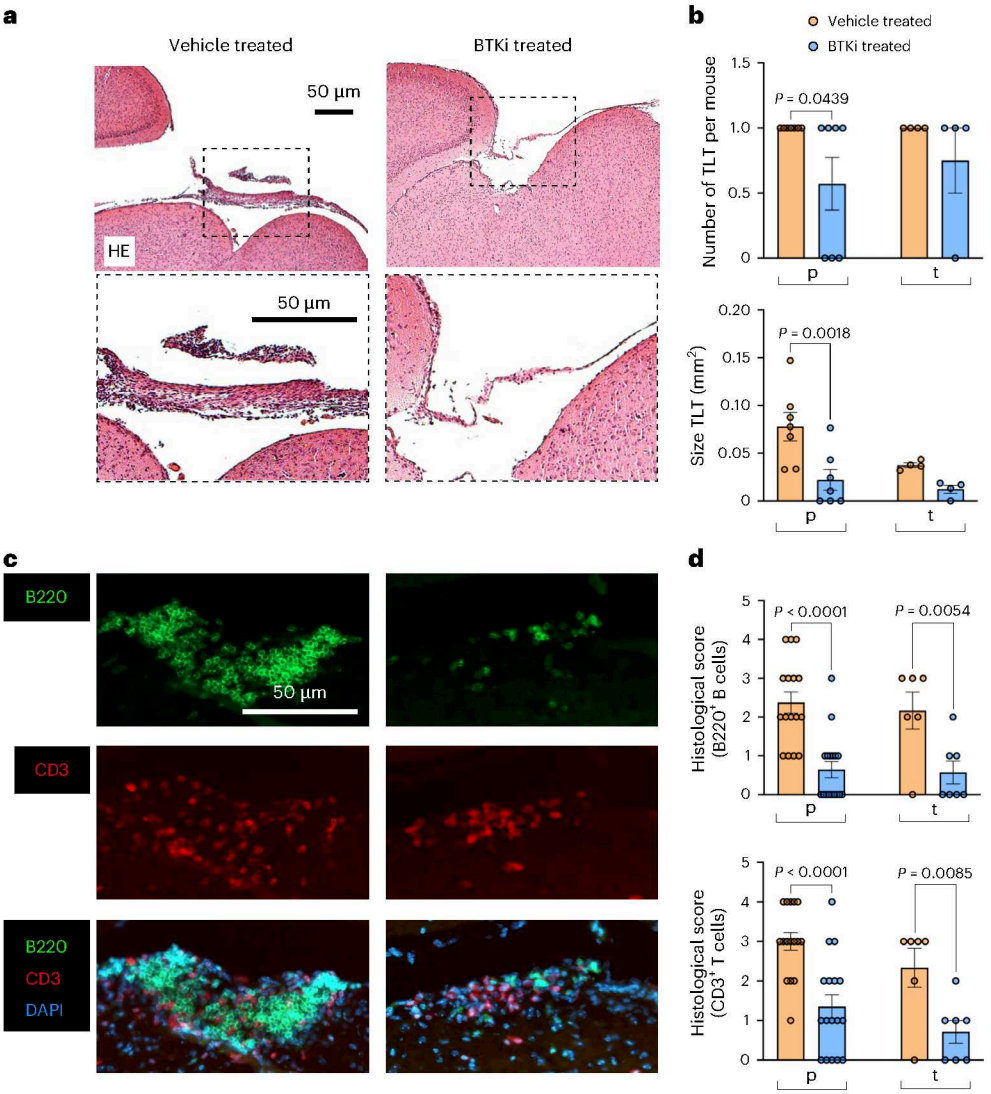

Fig. 3 | BTK inhibition reduces the size and number of B cell-rich leptomeningeal aggregates in SJL/J adoptive transfer EAE mice. **a**, Representative hematoxylin and eosin (HE)-stained sections of the leptomeninges overlaying the cortices of vehicle-treated or BTKi-treated SJL/J adoptive transfer EAE mice at peak disease (day 12 after adoptive transfer) with treatment administered in the therapeutic modality. **b**, The quantification of the number and size of leptomeningeal TLTs shown in p-vehicle treated ($n = 7$), p-BTKi-treated ($n = 7$), t-vehicle treated ($n = 4$) and t-BTKi-treated ($n = 4$) mice. **c**, Representative immunofluorescence images of leptomeninges stained for $B220^+$ B cells and $CD3^+$ T cells at peak disease. **d**, The histological scores of B and T cells shown in **c** (p-vehicle treated $n = 16$, p-BTKi treated $n = 17$, t-vehicle treated $n = 6$ and t-BTKi treated $n = 7$). Data are shown as mean ± s.e.m. Statistical analysis was conducted using a one-way ANOVA with multiple comparison. Experiments were performed three times with similar results.

Given our previous observation that LTβR signaling is required not only for expression of *Cxcl13* but also for the organization of B cells within TLT[2], we next asked whether CXCL13 levels correlated with accumulation of B cells in the leptomeninges in the different treatment groups (control, BTKi and BTKi + αLTβR). Indeed, BTKi treatment resulted in a reduction in the amount of B220 signal within the TLT, which was reversed by αLTβR agonist antibody administration (Fig. 6b), and a significant positive correlation was observed between B220 and CXCL13 staining within TLT (Fig. 6c).

Depletion of B cells with anti-CD20 therapy has been previously shown to augment levels of the B cell survival protein (B cell activating factor, BAFF) in the cerebrospinal fluid (CSF) of EAE mice and patients with MS, potentially because of the removal of the main BAFF-consuming cell type (B cells)[27]. Staining for BAFF by immunofluorescence revealed that it is expressed at a steady state in the leptomeninges of naive mice. However, during EAE, leptomeningeal BAFF expression is significantly reduced and only detected in areas that are relatively poor in $B220^+$ B cells. This paucity in BAFF was restored in the leptomeninges by BTKi treatment, but not in mice that received both BTKi and αLTβR agonist antibody treatment (Fig. 6d,e). Overall, a strong anti-correlation between B220 and BAFF staining was observed (Fig. 6f).

The disparate directionality of BAFF versus CXCL13 expression in leptomeninges in the various treatment groups led us to hypothesize that, on a per-mouse basis, these two molecules were potentially acting in opposition. To assess this, we examined the CXCL13:BAFF ratio for each animal. Vehicle-treated mice with prominent TLT exhibited a high CXCL13:BAFF ratio, whereas BTKi-treated mice with ablated TLT exhibited a low CXCL13:BAFF ratio, which was reversed with αLTβR treatment (Fig. 6g). Therefore, BTK inhibition significantly decreases the CXCL13:BAFF ratio in the leptomeninges of EAE mice in an LTβR-dependent manner, concomitant with abrogation of TLT formation.

Last, we asked if the accumulation of BAFF in the leptomeninges of BTKi-treated mice was causally associated with protection against subpial cortical gray matter pathology in EAE mice. To test this, we

https://doi.org/10.1038/s41590-025-02359-5

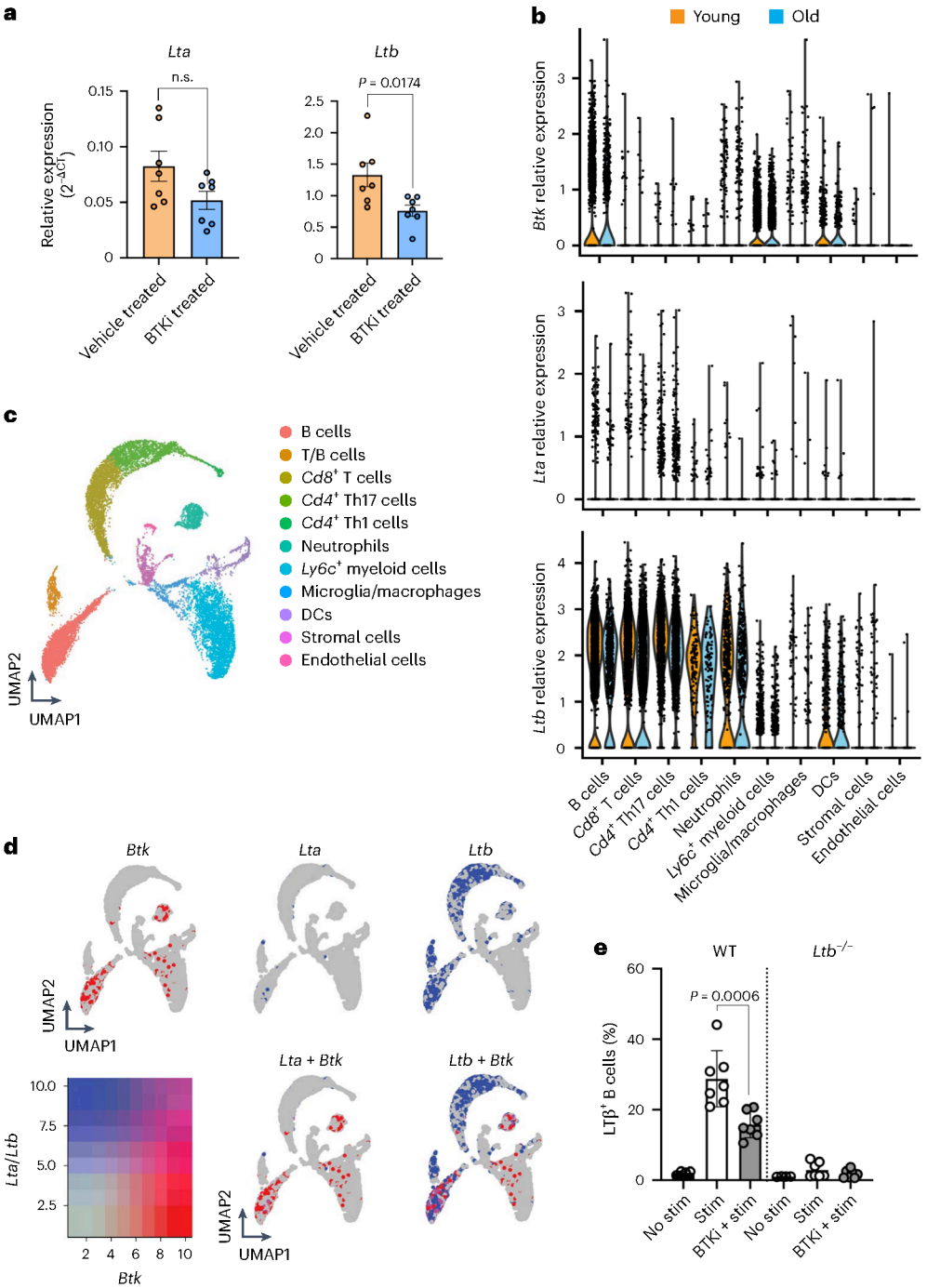

Fig. 4 | BTKi affects LTβR signaling in B cells. a, qPCR data of *Lta* and *Ltb* in the leptomeninges of vehicle-treated or BTKi-treated SJL/J adoptive transfer EAE mice at peak disease. **b**–**d**, scRNAseq of leptomeninges from young ($n = 2$) and old ($n = 2$) SJL/J mice at acute adoptive transfer EAE and appropriate age-matched, naive controls young and old EAE mice: violin plots showing relative gene expression of *Btk* and LT ligand genes (*Lta* and *Ltb*) in identified cell clusters stratified by age (**b**), a uniform manifold approximation and projection (UMAP) of 16,568 leptomeningeal cells after unsupervised clustering (**c**) and the gene co-expression of *Btk* with *Ltb* and *Lta* projected on the global UMAP (**d**). Data shown represent two biological and experimental repeats, each with $n = 1$ for each group analyzed. **e**, The flow cytometry of the LTβ-positive population in $CD19^+$ $B220^+$ B cells from naive (WT) SJL/J ($n = 7$) or $Ltb^{-/-}$ mice ($n = 7$) splenocytes stimulated with mouse anti-CD40 (5 μg ml^{-1}) + LPS (1 μg ml^{-1}) (stim) ex vivo or pretreated 1 h with BTKi (10 nM). Data in **a** and **e** are shown as mean ± s.d. Statistical analysis was conducted using two-sided unpaired *t*-tests for **a** and two-sided Mann–Whitney tests for **e**. n.s., not significant. $n = 7$ in each group.

administered an anti-BAFF mAb (αBAFF) at days 9 and 11 post-adoptive transfer of Th17 cells, concomitant with BTKi treatment. Combined BTK inhibition and αBAFF treatment reversed the beneficial effects conferred by BTKi, resulting in a restoration of glial limitans disruption, demyelination, microgliosis and axonal loss in the subpial gray matter (Fig. 7a–d). Therefore, BTKi-mediated protection against EAE-induced subpial gray matter injury is causally associated with a restoration of BAFF back to homeostatic levels in the leptomeninges.

In summary, BTKi treatment reduces leptomeningeal CXCL13 levels, B cell accumulation and TLT formation in an LTβR-dependent manner, corresponding with an increased level in leptomeningeal BAFF, which has the capacity to protect against cortical gray matter injury.

https://doi.org/10.1038/s41590-025-02359-5

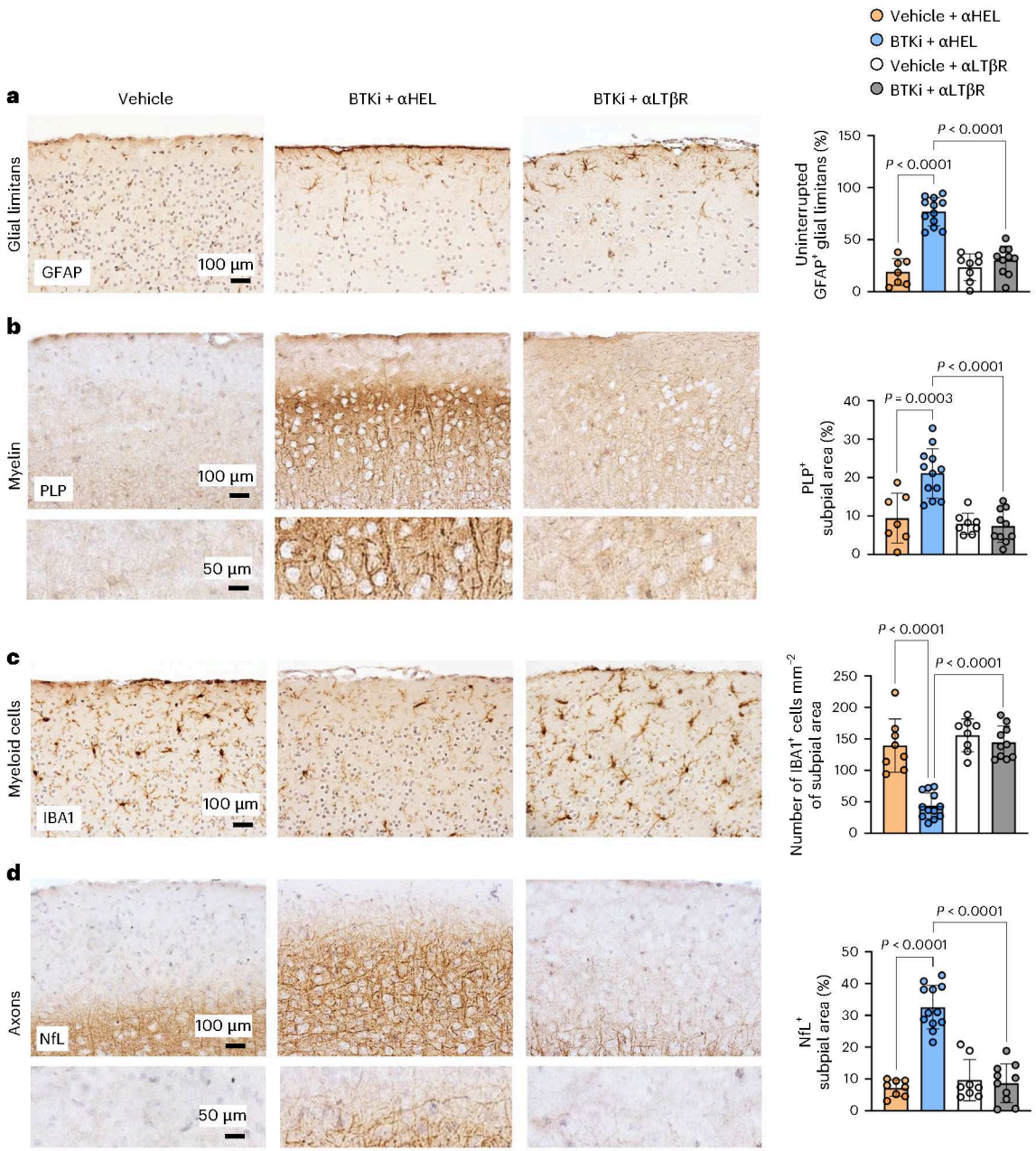

Fig. 5 | BTK inhibition prevents glial limitans disruption, gray matter demyelination, myeloid cell accumulation and axonal loss in the brain in a LT-dependent manner. Immunohistochemical staining and quantification of SSC tissue from vehicle-treated; BTKi-treated and αHEL-treated; or BTKi and αLTβR-treated SJL/J adoptive transfer EAE mice at peak disease (day 12 after adoptive transfer) for GFAP visualizing the glial limitans (**a**), PLP visualizing myelin (**b**), IBA1 visualizing microglia and macrophages (**c**), and NfL visualizing axons (**d**). Zoomed subpial areas are taken at equivalent depths from the pia mater across groups. Data are shown as mean ± s.d. Statistical analysis was conducted using one-way ANOVA. Vehicle and αHEL treated ($n = 7$), BTKi and αHEL treated ($n = 12$), vehicle and αLTβR treated ($n = 7$), and BTKi and αLTβR treated ($n = 8$).

A high CSF CXCL13:BAFF ratio reflects compartmentalized inflammation in MS

To test the relevance of our EAE findings in MS, we sourced a cohort of post mortem brain tissues from patients with MS from which matched CSF had also been collected at rapid autopsy (Supplementary Table 1). Importantly, we previously stratified these brain tissues into those with high versus low leptomeningeal B cell counts on the basis of the median level of B cell counts across the cohort, discovering that patients with high numbers of leptomeningeal B cells had larger subpial gray matter lesions as well as chronic active–inactive lesions[34]. We accessed the matched CSF from this cohort and used a sensitive ELISA-based method to measure the CXCL13:BAFF ratio in this compartment. We also measured CSF levels of neurofilament light chain (NfL) and glial fibrillary acidic protein (GFAP), fluid biomarkers that are used to monitor MS relapsing disease activity[35,36]. While CSF NfL and GFAP levels were not significantly different between patients with MS who showed evidence of high versus low levels of leptomeningeal B cells (Fig. 8a,b), the CXCL13:BAFF ratio in the CSF was significantly elevated in patients with MS who exhibited high numbers of leptomeningeal B cells compared with patients with MS who exhibited low numbers of leptomeningeal B cells (Fig. 8c).

Encouraged by these data, we next examined levels of NfL, GFAP and the CXCL13:BAFF ratio in the CSF of a cohort of living patients who exhibited MRI-confirmed paramagnetic rim lesion load (PRLs). PRLs

https://doi.org/10.1038/s41590-025-02359-5

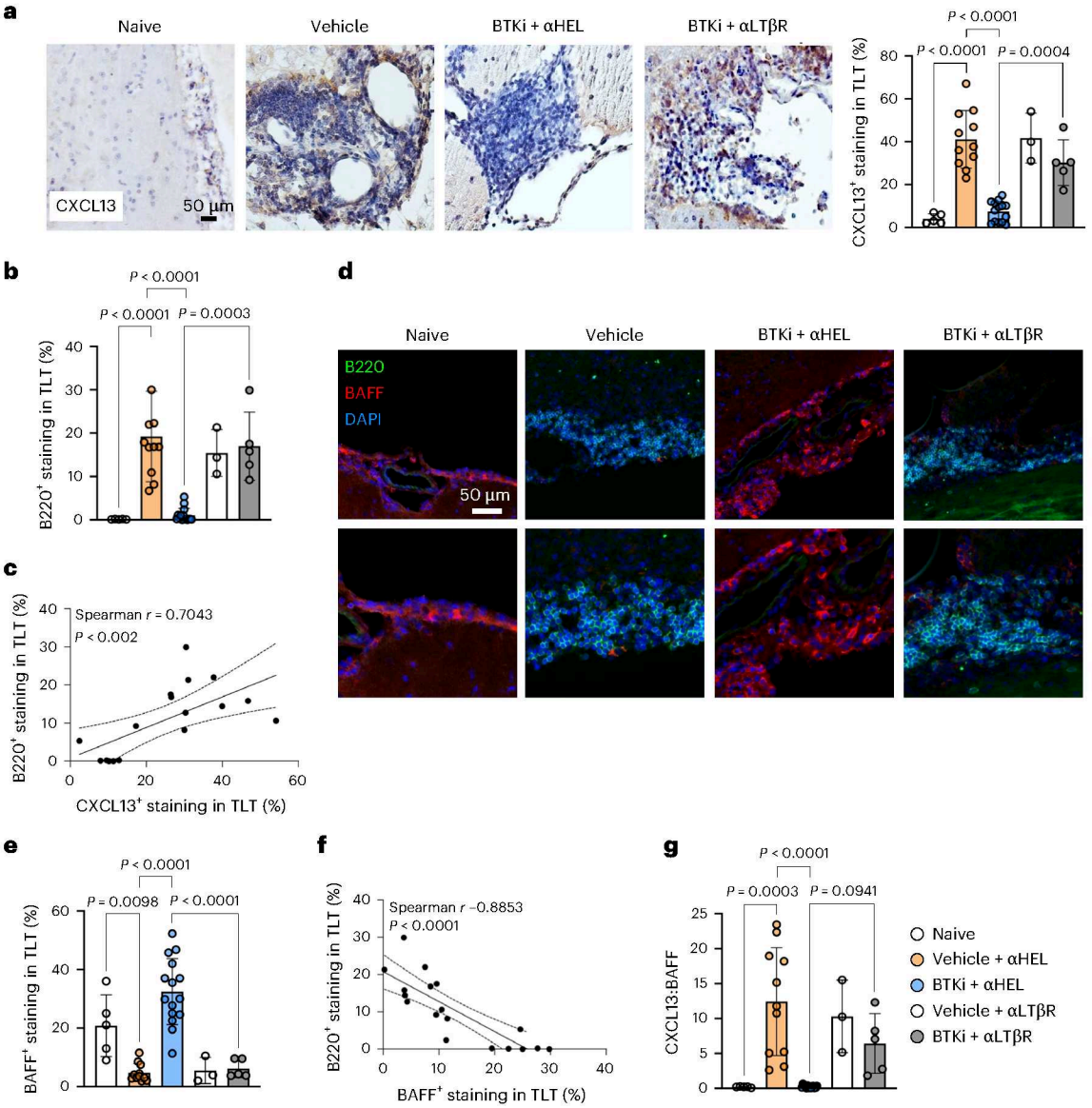

Fig. 6 | BTK inhibition reduces accumulation of CXCL13 and boosts the levels of BAFF in the leptomeninges in an LT-dependent manner. **a**, Representative immunohistochemical staining and quantification of CXCL13 in the leptomeninges of vehicle-treated; BTKi and αHEL-treated; or BTKi and αLTβR-treated SJL/J adoptive transfer EAE mice at peak disease (12 days after adoptive transfer). **b**, The quantification of B220$^+$ B cells in the leptomeninges of vehicle-treated; BTKi and αHEL-treated; or BTKi and αLTβR-treated SJL/J adoptive transfer EAE mice at peak disease. **c**, The correlation between the percentage of B220$^+$ B cell staining and the percentage of CXCL13$^+$ staining in the leptomeninges of vehicle-treated; BTKi and αHEL-treated; or BTKi and αLTβR-treated SJL/J adoptive transfer EAE mice at peak disease. **d**, Representative immunofluorescent staining of B220$^+$ B cells and BAFF in the leptomeninges of vehicle-treated; BTKi and αHEL-treated; or BTKi and αLTβR-treated SJL/J adoptive transfer EAE mice at peak disease. Nuclei are stained with DAPI. **e**, The quantification of BAFF in the leptomeninges of vehicle-treated; BTKi and αHEL-treated; or BTKi and αLTβR-treated SJL/J adoptive transfer EAE mice at peak disease. **f**, The correlation between the percentage of B220$^+$ B cells staining and the percentage of BAFF$^+$ staining in the leptomeninges of vehicle-treated; BTKi and αHEL-treated; or BTKi and αLTβR-treated SJL/J adoptive transfer EAE mice at peak disease. **g**, The CXCL13:BAFF ratio in the leptomeninges of vehicle-treated; BTKi and αHEL-treated; or BTKi and αLTβR-treated SJL/J adoptive transfer EAE mice at peak disease. Data are shown as mean ± s.d. Statistical analysis in **a**, **b**, **e** and **g** was conducted using one-way ANOVA. Correlation analysis in **d** and **f** was conducted using the two-sided nonparametric Spearman correlation coefficient.

are another measure of compartmentalized inflammation, which represent the in vivo imaging correlate of histologically defined chronic active white matter lesions[37–40] (Supplementary Table 1). We found that while CSF NfL and GFAP levels were not different between patients with MS with or without PRLs (Fig. 8d,e), the CXCL13:BAFF ratio in the CSF was significantly elevated in patients with MS with PRLs versus those patients without evidence of PRLs (Fig. 8f). In summary, these data indicate that a high CXCL13:BAFF ratio in the CSF is associated with elevated leptomeningeal B cells and PRLs in MS.

Discussion

The molecular mechanisms that underlie the formation and maintenance of TLTs are remarkably similar to that of secondary lymphoid organs, with both processes involving the LT pathway[41,42] and the production of B cell homing chemokines such as CXCL13[2,43]. Here, using remibrutinib, a selective covalent BTKi in phase 3 for MS[24], our study revealed a leptomeningeal circuitry that drives cortical injury in EAE. We found that the presence of leptomeningeal B cell-rich aggregates requires both BTK and LTβR signaling, and that these aggregates are

https://doi.org/10.1038/s41590-025-02359-5

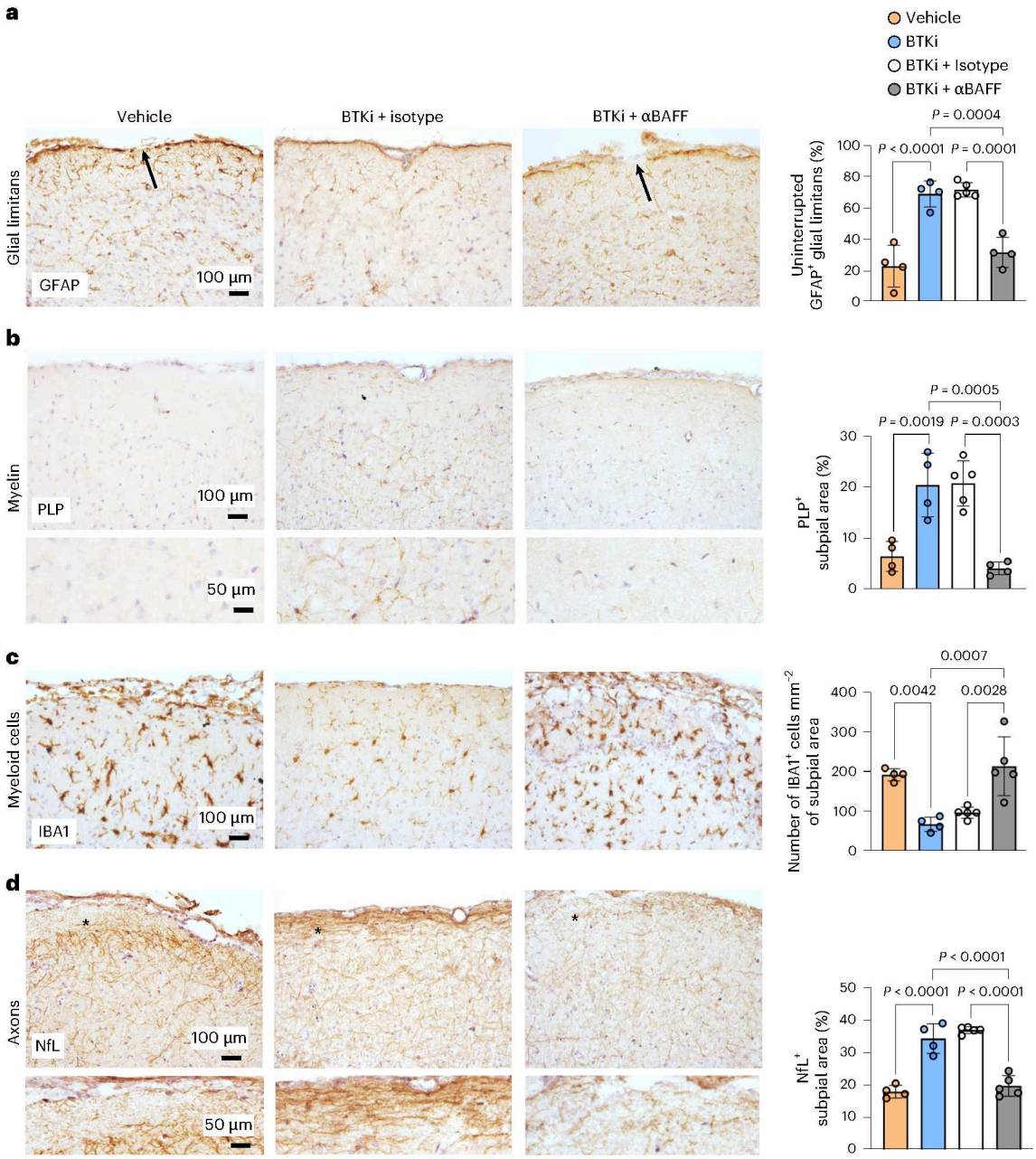

Fig. 7 | BTK inhibition spares the glial limitans and prevents cortical gray matter demyelination, myeloid cell accumulation and axonal loss in young SJL/J adoptive transfer EAE mice in a BAFF-dependent manner. **a**–**d**, Immunohistochemical staining and quantification of SSC tissue from vehicle-treated, BTKi-treated, BTKi + isotype-treated and BTKi + αBAFF-treated SJL/J adoptive transfer EAE mice at peak disease (day 12 after adoptive transfer) for GFAP visualizing the glial limitans (**a**), PLP visualizing myelin (**b**), IBA1 visualizing microglia and macrophages (**c**), and NfL visualizing axons (**d**). Zoomed subpial areas are taken at equivalent depths from the pia mater across groups. Black arrows in **a** indicate disrupted glial limitans. Data are shown as mean ± s.d. Statistical analysis was conducted using one-way ANOVA. Vehicle treated ($n = 4$), BTKi treated ($n = 4$), BTKi + isotype treated ($n = 5$) and BTKi + αBAFF treated ($n = 5$).

associated with low levels of BAFF and high levels of CXCL13 within the leptomeninges. In addition, the underlying cortical pathology in Th17-induced EAE mice was prevented by BTKi even upon therapeutic treatment of aged mice, which normally exhibit non-remitting gray matter injury and brain volume loss[17]. In patients with MS, a high CXCL13:BAFF ratio in the CSF was associated with a greater degree of compartmentalized inflammation.

BTKi had no significant effect on spinal cord demyelination in our model. This is not surprising as the method of EAE induction is fundamentally different in the passive SJL/J EAE model compared to the active C57Bl/6 model used in other studies[20,22,23], where antigen persists in the form of an adjuvant depot. We hypothesize that since adoptively transferred Th17 cells enter the leptomeninges before B cells[2], the therapeutic impact of B cell depletion[27] and BTKi is too late to impact this initial inflammatory acute phase of disease. Indeed, we found that the T cells that infiltrate the leptomeninges in BTKi-treated mice show no appreciable changes in intracellular interferon-γ (IFN-γ), interleukin-17A (IL-17A) or granulocyte-macrophage colony-stimulating factor (GM-CSF) expression compared to vehicle treated mice (Extended Data Fig. 8). This also implies that, once primed,

https://doi.org/10.1038/s41590-025-02359-5

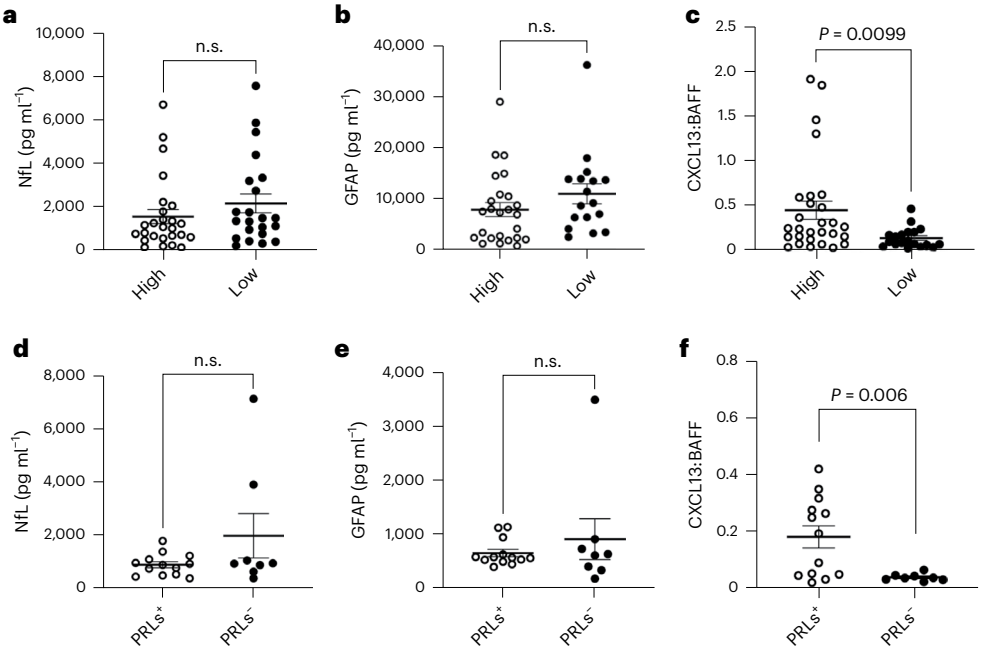

Fig. 8 | An elevated CXCL13:BAFF ratio in the CSF is associated with compartmentalized inflammation in MS. a–**f**, The quantification of NfL (**a** and **d**), GFAP (**b** and **e**) and CXCL13 and BAFF (**c** and **f**) by ELISA-based methods in CSF collected post mortem from MS donors with high ($n = 25$) versus low ($n = 22$) meningeal CD20$^+$ B cell count (**a**–**c**) or in CSF collected from a living cohort of patients with MS with ($n = 13$) or without ($n = 8$) PRLs (**d**–**f**). Data are shown as mean ± s.d. Statistical analysis was conducted using two-sided Mann–Whitney tests (**a**–**c**) or analysis of covariance (**d**–**f**).

T cells play a minimal role in driving cortical injury. In agreement, scRNAseq of the leptomeninges of aged SJL/J mice, which, compared to young (remitting) SJL/J EAE mice, exhibit severe EAE and cortical shrinkage, revealed very limited differences in gene expression in T cells compared to B cells[17]. In support, we recently showed that B cells are a key determinant of gray matter pathology in this model, as anti-CD20 B cell depletion therapy prevents pathology[27].

We previously found that the B cell chemokine *Cxcl13* accumulates in the leptomeninges in response to Th17 cells[2]. In line with the high local expression of CXCL13 in the inflamed EAE leptomeninges, CXCL13 has also been detected in the CSF of post mortem MS cases with high levels of meningeal inflammation and gray matter demyelination[44]. Several proinflammatory cytokines (IFN-γ, TNF, IL-2 and IL-22) and other molecules (CXCL10, LTα, IL-6 and IL-10) have been detected together with CXCL13 in the CSF[44], suggesting an environment of sustained B cell activity and lymphoid-neogenesis in MS cases with high levels of leptomeningeal inflammation. Here we show that enforced LTβR signaling can restore high levels of CXCL13 in the leptomeninges in BTKi-treated mice, suggesting that this signal lies downstream of BTK. A positive feedback loop involving CXCR5-mediated induction of $LT\alpha_1\beta_2$ expression by B cells is required for optimal B cell organization in the spleen[45]. We propose that a similar positive feedback loop mediates accumulation of B cells in leptomeninges, which indirectly results in an augmentation of CXCL13 production by stromal cells via LTβR signaling.

Interestingly, we noted that the accumulation of CXCL13 and B cells negatively correlated with the amount of BAFF in the EAE leptomeninges. We previously showed that high BAFF levels induced by anti-CD20 treatment are neuroprotective in MS and EAE[27]. Moreover, MS disease activity is exacerbated in patients treated with atacicept, a soluble TACI decoy receptor that binds and neutralizes BAFF[46]. Although treatment with BTKi does not deplete B cells[47] we did nevertheless notice a substantial reduction in the amount and organization of B cells within vestigial TLTs. A potential mechanism of action of BTKi in preventing cortical pathology may therefore be via increased local levels of BAFF. As we showed previously, BAFF may act by promoting survival of stressed neurons[27], in agreement with its neuroprotective effects previously described[48,49], although this is probably not the only mechanism of action of BAFF in the leptomeninges. We have previously shown that *Tnfsf13b* is primarily expressed by myeloid cells in the leptomeninges of SJL/J EAE[17]. Given that B cells are the major consumers of BAFF, a reduction in B cell numbers should increase the availability of BAFF, as demonstrated in ref. 27; although, whether myeloid cells (or other cells) further contribute to the pool of available BAFF remains possible. Therefore, according to our model, T cells initiate TLT formation, whereas B cells maintain TLT via the LT pathway while causing pathology owing to their consumption of BAFF, which under homeostatic conditions is important for neuroprotection in the underlying gray matter.

Consistent with our model, we noted that in EAE, the CXCL13:BAFF ratio was high in mice with leptomeningeal inflammation and cortical injury (vehicle treatment or BTKi treatment with LTβR stimulation) and low in mice which were spared these outcomes (BTKi-treated without LTβR stimulation). We therefore hypothesized that the CXCL13:BAFF ratio may be used as a proxy for B cell-rich TLTs in MS. Indeed, we found that the CXCL13:BAFF ratio was high in the CSF of patients with MS and high levels of leptomeningeal B cells compared to those with low levels of leptomeningeal B cells. Identifying and tracking meningeal inflammation in living patients—which could be used to monitor the effect of interventions targeting TLTs—is challenging. While contrast-enhanced fluid-attenuated inversion recovery (FLAIR) imaging[12] and, more recently, 7T MRI[50,51] have the capacity to visualize leptomeningeal enhancement, whether this represents TLTs or scar tissue resulting from stromal cell remodeling underpinning these structures[52,53], remains unclear[54].

Using the same post mortem brain tissue, we had previously shown that the proportion of chronic active white matter lesions positively correlates with the extent of leptomeningeal inflammation[34]. The mechanistic link between chronic active white matter lesions and leptomeningeal inflammation could be potentially caused by augmented myelin antigen priming of T cells in the periphery that subsequently migrate to the leptomeninges[55] or owing to retrograde degeneration propagating backward toward cortical neurons, resulting in the formation

of gray matter lesions, as supported by linked damage in these two compartments[56–59]. Regardless of the mechanism, B cell-rich leptomeningeal aggregates accumulate in patients with MS with a higher proportion of chronic active white matter lesions[34]. Using this knowledge, we elected to examine the relationship between CXCL13:BAFF ratios in the CSF and PRLs, the radiological equivalent of chronic active white matter lesions[40]. Remarkably, high CSF CXCL13:BAFF ratios, but not CSF levels of NfL or GFAP, were associated with the presence of PRLs in patients with MS. Thus, we propose that measuring CXCL13:BAFF ratios in the CSF can help identify patients with compartmentalized inflammation, which includes both leptomeningeal TLT and PRLs, enabling better patient stratification and treatment monitoring. By extension, we predict that patients with MS who have a high CXCL13:BAFF ratio in the CSF may particularly benefit from treatment with BTKi.

There are some limitations to our study. In addition to B cells, myeloid cells express BTK and could be the target of BTKi[20,60,61]. Since our choice of the SJL/J model was predicated on our quest to understand how BTK inhibitors impact cortical gray matter pathology, we are consequently limited by the lack of genetic tools in the SJL/J background that would isolate the impact of BTKi on specific immune cell types in the LM. Ideally an experiment that silences BTK in myeloid versus B cells in vivo would complement our findings. Nevertheless, in the absence of such tools, we can draw some interpretations from our scRNAseq findings. Unlike B cells, myeloid cells do not co-express both *Ltb* and *Lta*, and thus cannot provide a signal to LTβR expressing cells. Therefore, despite our finding that *Btk* is expressed in leptomeningeal myeloid cells, BTK signaling in myeloid cells is not necessary for leptomeningeal inflammation and cortical pathology as this can proceed in the presence of BTK inhibition when the LT pathway is agonized, although a role for myeloid cell-intrinsic BTK in gray matter pathology independent of LTβR signaling remains possible. We also recognize that our characterization of myeloid cells in tissue do not necessarily distinguish microglial cells from macrophages, which is challenging to do in situ[62]. Last, we have not unraveled the signaling pathway that leads to BTK-dependent upregulation of LTαβ in the LM. We previously showed that ICOS-dependent CD40 ligand expression on $CD4^+$ T cells triggers the upregulation of LTαβ on B cells in the spleen[63]. Since we show here that BTKi reduces LTαβ upregulation in response to CD40 stimulation, this suggests that BTKi, which has been shown to operate downstream of CD40[64,65], may promote B cell intrinsic LTαβ expression by influencing CD40 signaling, although this remains to be tested. Proving this in vivo would be tricky as it would require blockade of CD40 ligand, which will likely have other impacts beyond LTαβ expression.

In summary, our study reveals a novel BTK-dependent circuit that establishes B cell-rich TLT in the leptomeninges during EAE, demonstrates that dissolving these structures ameliorates gray matter injury in a BAFF-dependent manner and links high CXCL13:BAFF ratios in the CSF with compartmentalized inflammation in patients with MS. Future studies should characterize the impact of BTKi on CXCL13:BAFF ratios in patients with MS and on leptomeningeal/CSF B cell phenotype.

Online content

Any methods, additional references, Nature Portfolio reporting summaries, source data, extended data, supplementary information, acknowledgements, peer review information; details of author contributions and competing interests; and statements of data and code availability are available at https://doi.org/10.1038/s41590-025-02359-5.

References

1. Aloisi, F. & Pujol-Borrell, R. Lymphoid neogenesis in chronic inflammatory diseases. *Nat. Rev. Immunol.* **6**, 205–217 (2006).
2. Pikor, N. B. et al. Integration of Th17- and lymphotoxin-derived signals initiates meningeal-resident stromal cell remodeling to propagate neuroinflammation. *Immunity* **43**, 1160–1173 (2015).
3. Serafini, B., Rosicarelli, B., Magliozzi, R., Stigliano, E. & Aloisi, F. Detection of ectopic B-cell follicles with germinal centers in the meninges of patients with secondary progressive multiple sclerosis. *Brain Pathol.* **14**, 164–174 (2004).
4. Bevan, R. J. et al. Meningeal inflammation and cortical demyelination in acute multiple sclerosis. *Ann. Neurol.* **84**, 829–842 (2018).
5. Howell, O. W. et al. Meningeal inflammation is widespread and linked to cortical pathology in multiple sclerosis. *Brain* **134**, 2755–2771 (2011).
6. Magliozzi, R. et al. A gradient of neuronal loss and meningeal inflammation in multiple sclerosis. *Ann. Neurol.* **68**, 477–493 (2010).
7. Magliozzi, R. et al. B-cell enrichment and Epstein–Barr virus infection in inflammatory cortical lesions in secondary progressive multiple sclerosis. *J. Neuropathol. Exp. Neurol.* **72**, 29–41 (2013).
8. Magliozzi, R. et al. Meningeal B-cell follicles in secondary progressive multiple sclerosis associate with early onset of disease and severe cortical pathology. *Brain* **130**, 1089–1104 (2007).
9. Lucchinetti, C. F. et al. Inflammatory cortical demyelination in early multiple sclerosis. *N. Engl. J. Med.* **365**, 2188–2197 (2011).
10. Makshakov, G. et al. Leptomeningeal contrast enhancement is associated with disability progression and grey matter atrophy in multiple sclerosis. *Neurol. Res. Int.* **2017**, 8652463 (2017).
11. Titelbaum, D. S. et al. Leptomeningeal enhancement on 3D-FLAIR MRI in multiple sclerosis: systematic observations in clinical practice. *J. Neuroimaging* **30**, 917–929 (2020).
12. Absinta, M. et al. Gadolinium-based MRI characterization of leptomeningeal inflammation in multiple sclerosis. *Neurology* **85**, 18–28 (2015).
13. Kappos, L. et al. Ocrelizumab in relapsing-remitting multiple sclerosis: a phase 2, randomised, placebo-controlled, multicentre trial. *Lancet* **378**, 1779–1787 (2011).
14. Steinman, L. Immunology of relapse and remission in multiple sclerosis. *Annu. Rev. Immunol.* **32**, 257–281 (2014).
15. Bo, L., Geurts, J. J., Mork, S. J. & van der Valk, P. Grey matter pathology in multiple sclerosis. *Acta Neurol. Scand. Suppl.* **183**, 48–50 (2006).
16. Peters, A. et al. Th17 cells induce ectopic lymphoid follicles in central nervous system tissue inflammation. *Immunity* **35**, 986–996 (2011).
17. Zuo, M. et al. Age-dependent gray matter demyelination is associated with leptomeningeal neutrophil accumulation. *JCI Insight* **7** (2022).
18. Ward, L. A. et al. Siponimod therapy implicates Th17 cells in a preclinical model of subpial cortical injury. *JCI Insight* **5** (2020).
19. Angst, D. et al. Discovery of LOU064 (remibrutinib), a potent and highly selective covalent inhibitor of Bruton's tyrosine kinase. *J. Med. Chem.* **63**, 5102–5118 (2020).
20. Nuesslein-Hildesheim, B. et al. Remibrutinib (LOU064) inhibits neuroinflammation driven by B cells and myeloid cells in preclinical models of multiple sclerosis. *J. Neuroinflammation* **20**, 194 (2023).
21. Hao, Y. et al. Dictionary learning for integrative, multimodal and scalable single-cell analysis. *Nat. Biotechnol.* **42**, 293–304 (2024).
22. Bhargava, P. et al. Imaging meningeal inflammation in CNS autoimmunity identifies a therapeutic role for BTK inhibition. *Brain* **144**, 1396–1408 (2021).
23. Evonuk, K. S. et al. Bruton's tyrosine kinase inhibition reduces disease severity in a model of secondary progressive autoimmune demyelination. *Acta Neuropathol. Commun.* **11**, 115 (2023).

24. Kramer, J., Bar-Or, A., Turner, T. J. & Wiendl, H. Bruton tyrosine kinase inhibitors for multiple sclerosis. *Nat. Rev. Neurol.* **19**, 289–304 (2023).
25. Siffrin, V. et al. In vivo imaging of partially reversible Th17 cell-induced neuronal dysfunction in the course of encephalomyelitis. *Immunity* **33**, 424–436 (2010).
26. Langrish, C. L. et al. IL-23 drives a pathogenic T cell population that induces autoimmune inflammation. *J. Exp. Med.* **201**, 233–240 (2005).
27. Wang, A. A. et al. B cell depletion with anti-CD20 promotes neuroprotection in a BAFF-dependent manner in mice and humans. *Sci. Transl. Med.* **16**, eadi0295 (2024).
28. Absinta, M., Lassmann, H. & Trapp, B. D. Mechanisms underlying progression in multiple sclerosis. *Curr. Opin. Neurol.* **33**, 277–285 (2020).
29. Calabrese, M. et al. The changing clinical course of multiple sclerosis: a matter of gray matter. *Ann. Neurol.* **74**, 76–83 (2013).
30. Florescu, A. et al. Dynamic alterations of dural and bone marrow B cells in an animal model of progressive multiple sclerosis. *J. Exp. Med.* **222** (2025).
31. Gommerman, J. L. & Browning, J. L. Lymphotoxin/light, lymphoid microenvironments and autoimmune disease. *Nat. Rev. Immunol.* **3**, 642–655 (2003).
32. Kuprash, D. V. et al. Cyclosporin A blocks the expression of lymphotoxin alpha, but not lymphotoxin beta, in human peripheral blood mononuclear cells. *Blood* **100**, 1721–1727 (2002).
33. Rennert, P. D., James, D., Mackay, F., Browning, J. L. & Hochman, P. S. Lymph node genesis is induced by signaling through the lymphotoxin beta receptor. *Immunity* **9**, 71–79 (1998).
34. Ahmed, S. M. et al. Accumulation of meningeal lymphocytes correlates with white matter lesion activity in progressive multiple sclerosis. *JCI Insight* **7** (2022).
35. Benkert, P. et al. Serum neurofilament light chain for individual prognostication of disease activity in people with multiple sclerosis: a retrospective modelling and validation study. *Lancet Neurol.* **21**, 246–257 (2022).
36. Abdelhak, A., Huss, A., Kassubek, J., Tumani, H. & Otto, M. Author correction: serum GFAP as a biomarker for disease severity in multiple sclerosis. *Sci. Rep.* **9**, 8433 (2019).
37. Absinta, M. et al. A lymphocyte–microglia–astrocyte axis in chronic active multiple sclerosis. *Nature* **597**, 709–714 (2021).
38. Maggi, P. et al. Paramagnetic rim lesions are specific to multiple sclerosis: an international multicenter 3T MRI study. *Ann. Neurol.* **88**, 1034–1042 (2020).
39. Motamedgorji, N. et al. Characterizing iron rim lesions in multiple sclerosis: a biomarker for disease activity and progression: a systematic review and meta-analysis. *Neuroradiology* (2025).
40. Dal-Bianco, A., Oh, J., Sati, P. & Absinta, M. Chronic active lesions in multiple sclerosis: classification, terminology, and clinical significance. *Ther. Adv. Neurol. Disord.* **17**, 17562864241306684 (2024).
41. Drayton, D. L., Ying, X., Lee, J., Lesslauer, W. & Ruddle, N. H. Ectopic LT alpha beta directs lymphoid organ neogenesis with concomitant expression of peripheral node addressin and a HEV-restricted sulfotransferase. *J. Exp. Med.* **197**, 1153–1163 (2003).
42. Lu, T. T. & Browning, J. L. Role of the lymphotoxin/LIGHT system in the development and maintenance of reticular networks and vasculature in lymphoid tissues. *Front. Immunol.* **5**, 47 (2014).
43. Cupedo, T. & Mebius, R. E. Role of chemokines in the development of secondary and tertiary lymphoid tissues. *Semin. Immunol.* **15**, 243–248 (2003).
44. Magliozzi, R. et al. Inflammatory intrathecal profiles and cortical damage in multiple sclerosis. *Ann. Neurol.* **83**, 739–755 (2018).
45. Ansel, K. M. et al. A chemokine-driven positive feedback loop organizes lymphoid follicles. *Nature* **406**, 309–314 (2000).
46. Kappos, L. et al. Atacicept in multiple sclerosis (ATAMS): a randomised, placebo-controlled, double-blind, phase 2 trial. *Lancet Neurol.* **13**, 353–363 (2014).
47. Haselmayer, P. et al. Efficacy and pharmacodynamic modeling of the BTK inhibitor evobrutinib in autoimmune disease models. *J. Immunol.* **202**, 2888–2906 (2019).
48. Kannel, K. et al. Changes in blood B cell-activating factor (BAFF) levels in multiple sclerosis: a sign of treatment outcome. *PLoS ONE* **10**, e0143393 (2015).
49. Rojas, O. L. et al. Recirculating intestinal IgA-producing cells regulate neuroinflammation via IL-10. *Cell* **176**, 610–624 e618 (2019).
50. Harrison, D. M. et al. Leptomeningeal enhancement at 7T in multiple sclerosis: frequency, morphology, and relationship to cortical volume. *J. Neuroimaging* **27**, 461–468 (2017).
51. Zurawski, J. et al. 7T MRI cerebral leptomeningeal enhancement is common in relapsing-remitting multiple sclerosis and is associated with cortical and thalamic lesions. *Mult. Scler.* **26**, 177–187 (2020).
52. Ramaglia, V., Florescu, A., Zuo, M., Sheikh-Mohamed, S. & Gommerman, J. L. Stromal cell-mediated coordination of immune cell recruitment, retention, and function in brain-adjacent regions. *J. Immunol.* **206**, 282–291 (2021).
53. Ramaglia, V., Rojas, O., Naouar, I. & Gommerman, J. L. The ins and outs of central nervous system inflammation-lessons learned from multiple sclerosis. *Annu Rev. Immunol.* **39**, 199–226 (2021).
54. Ighani, M. et al. No association between cortical lesions and leptomeningeal enhancement on 7-tesla MRI in multiple sclerosis. *Mult. Scler.* **26**, 165–176 (2020).
55. Stern, J. N. et al. B cells populating the multiple sclerosis brain mature in the draining cervical lymph nodes. *Sci. Transl. Med.* **6**, 248ra107 (2014).
56. Roosendaal, S. D. et al. Grey matter volume in a large cohort of MS patients: relation to MRI parameters and disability. *Mult. Scler.* **17**, 1098–1106 (2011).
57. Furby, J. et al. Different white matter lesion characteristics correlate with distinct grey matter abnormalities on magnetic resonance imaging in secondary progressive multiple sclerosis. *Mult. Scler.* **15**, 687–694 (2009).
58. Sanfilipo, M. P., Benedict, R. H., Sharma, J., Weinstock-Guttman, B. & Bakshi, R. The relationship between whole brain volume and disability in multiple sclerosis: a comparison of normalized gray vs. white matter with misclassification correction. *NeuroImage* **26**, 1068–1077 (2005).
59. De Stefano, N. et al. Evidence of early cortical atrophy in MS: relevance to white matter changes and disability. *Neurology* **60**, 1157–1162 (2003).
60. Gruber, R. C. et al. BTK regulates microglial function and neuroinflammation in human stem cell models and mouse models of multiple sclerosis. *Nat. Commun.* **15**, 10116 (2024).
61. Langlois, J. et al. Fenebrutinib, a Bruton's tyrosine kinase inhibitor, blocks distinct human microglial signaling pathways. *J. Neuroinflammation* **21**, 276 (2024).
62. Kim, J. S. et al. Clonal hematopoiesis-associated motoric deficits caused by monocyte-derived microglia accumulating in aging mice. *Cell Rep.* **44**, 115609 (2025).
63. Vu, F., Dianzani, U., Ware, C. F., Mak, T. & Gommerman, J. L. ICOS, CD40, and lymphotoxin beta receptors signal sequentially and interdependently to initiate a germinal center reaction. *J. Immunol.* **180**, 2284–2293 (2008).
64. Kil, L. P. et al. Btk levels set the threshold for B-cell activation and negative selection of autoreactive B cells in mice. *Blood* **119**, 3744–3756 (2012).

65. Brunner, C., Avots, A., Kreth, H. W., Serfling, E. & Schuster, V. Bruton's tyrosine kinase is activated upon CD40 stimulation in human B lymphocytes. *Immunobiology* **206**, 432–440 (2002).

[1]Department of Immunology, University of Toronto, Toronto, Ontario, Canada. [2]Translational Neuroradiology Section, National Institute of Neurological Disorders and Stroke, National Institutes of Health, Bethesda, MD, USA. [3]Department of Neurology, University Hospital of Basel and University of Basel, Basel, Switzerland. [4]Departments of Biomedicine and Clinical Research, University Hospital of Basel and University of Basel, Basel, Switzerland. [5]Research Center for Clinical Neuroimmunology and Neuroscience Basel, University Hospital of Basel and University of Basel, Basel, Switzerland. [6]Center of Neurology, Department of Neuroimmunology, University Hospital and University Bonn, Bonn, Germany. [7]German Center for Neurodegenerative Diseases, Bonn, Germany. [8]Mouse Imaging Centre, Hospital for Sick Children, Toronto, Ontario, Canada. [9]Novartis BioMedical Research, Basel, Switzerland. [10]Department of Virology, Immunology and Microbiology, Boston University Chobanian and Avedisian School of Medicine, Boston, MA, USA. [11]Krembil Brain Institute, University Health Network, Toronto, Ontario, Canada. ✉e-mail: jen.gommerman@utoronto.ca; valeria.ramaglia@uhn.ca

Methods

Post mortem human tissue retrieval

Tissue blocks for this study were obtained from the Netherlands Brain Bank. For the characterization of leptomeningeal immune cells, tissue blocks from 22 donors with progressive (primary progressive or secondary progressive) MS were selected on the basis of the presence of leptomeninges adjacent to the cortex in the tissue blocks. Tissue blocks were dissected on the basis of the identification of lesions, as guided by macroscopical examination and/or by post mortem MRI (since 2001) of 1-cm-thick coronal brain slices[66]. The tissue blocks used for the analysis of leptomeningeal inflammation and subpial demyelination performed in this study were dissected from the supratentorial cortex at locations that included the occipital or the parietal or the temporal or the frontal lobes. Matched CSF was obtained from the Netherlands Brain Bank. Detailed clinical–pathological and demographic data of all donors are provided in Supplementary Table 1. The age at the time of death of patients with MS ranged from 41 to 89 years (median 61.5 years), with a mean post mortem delay of 8 h 14 min (s.d. of 2 h 3 min). The clinical diagnosis of MS and its clinical course were determined by a certified neurologist and confirmed by a certified neuropathologist on the basis of the neuropathological analysis of the patient's brain autopsy. Tissue samples were obtained from patients with MS and controls with approval of the Vrije Universiteit Medical Center Review Board, who has reviewed and agreed with the procedures of the Netherlands Brain Bank concerning the 'donation of brain material for scientific research'. All patients signed informed consent. Where it concerns persons who, for reasons of their health, were unable to give informed consent (incompetent persons), informed authorization was obtained from the legal representative as defined in the Netherlands Civil Code (Burgerlijk Wetboek). The use of post mortem study was also approved by the University of Toronto (protocol number 30813).

Immunohistochemistry of post mortem human tissue

For the classification of cortical gray matter lesions, sections were stained by immunohistochemistry for the PLP marker of myelin. Leptomeningeal immune cells were identified by immunohistochemistry for CD3 to detect T cells and CD20 to detect B cells (Supplementary Table 2). Immunohistochemistry was performed as previously described[67,68]. Sections of 7 µm thickness were cut from formalin-fixed paraffin-embedded (FFPE) tissue blocks, collected on Superfrost Plus glass slides (VWR international) and dried overnight at 37 °C. Sections were deparaffinized in xylene (2 × 15 min) and rehydrated through a series (100%, 70% and 50%) of ethanol. Endogenous peroxidase activity was blocked by incubation in methanol (Merck KGaA) with 0.3% H_2O_2 (Merck KGaA) for 20 min at 21 °C. Sections were then rinsed in PBS and pretreated with microwave antigen retrieval (3 min at 900 W followed by 10 min at 90 W) in either 0.05 M Tris-buffered saline (pH 7.6) or 10 mM Tris 1 mM EDTA buffer pH 9.0 (Supplementary Table 2). Sections were incubated overnight at 4 °C in the appropriate primary antibody (Supplementary Table 2) diluted in Normal Antibody Diluent (Immunologic) and the next day with the BrightVision poly-HRP-Anti Ms/Rb/Rt IgG biotin-free (diluted 1:1 in PBS; Immunologic) for 30 min at 21 °C. The immunostaining was visualized with DAB (Vector Laboratories) for 4 min at 21 °C, and sections were counterstained with hematoxylin (Sigma Chemie GmbH), dehydrated in ethanol and mounted with Pertex (Histolab).

Quantification of subpial demyelination and leptomeningeal inflammation of post mortem human tissue

For the quantification of subpial demyelination, brain slides stained for PLP identifying myelin were used. Subpial (type III) lesions—which span from the pial surface typically to cortical layers 2–4—were imaged at original magnification 5× using a light microscope (Axioscope) connected to a digital camera (AxioCam MRc) and Zen pro 2.0 imaging software. The RGB images were separated into single-color channels using the color deconvolution plugin in ImageJ Pro Plus 7.0 imaging software (MediaCybernetics). The single-color channel for PLP was subjected to thresholding to create a mask that captured the specific staining. The area fraction measurement was applied to each image to quantify the percentage of thresholded staining. The scale represents the percentage of PLP^+ subpial cortical area in each brain section examined. For the quantification of leptomeningeal inflammation, leptomeningeal segments were randomly selected for imaging at 20× original magnification with a light microscope (Olympus BX41TF) connected to the Cell D software (Olympus). Immune cells were quantified in leptomeningeal areas that were adjacent to type III (subpial) gray matter lesions and in areas that were adjacent to normal appearing gray matter. A total of 71 ± 20% (mean ± s.d.) of intact leptomeninges were available for scoring in the MS cohort. $CD20^+$ B cell counts were done over a total leptomeningeal area of 47.53 mm^2 from patients with MS, of which 37.02 mm^2 was adjacent to gray matter lesions, 10.51 mm^2 was adjacent to normal appearing gray matter and 5.652 mm^2 of leptomeningeal area was adjacent to non-neurological control cortex. The leptomeningeal area (in square millimeters) was measured using the 'measurement' function of the Image Pro Plus 7.0 imaging software. Cell numbers were expressed as mean number per millimeter of intact leptomeninges. Considering the large dynamic range of the meningeal count for $CD20^+$ B cells (range of 0.89–16.27 cells per millimeter of meninges) in MS cases, the median was chosen as a cutoff to stratify the MS cases in those with high (above the median) or low (below the median) meningeal lymphocyte count (7.30 cells per millimeter for B cells)[34]. Since B cells are a proxy of leptomeningeal inflammation[3], the B cell cutoff was used in this study to stratify donors with high versus low leptomeningeal inflammation.

NIH cohort and metadata

The Ella-based proteomic data for the National Institutes of Health (NIH) cohort were collected following the approval of the institutional review board, and after written consent was obtained as part of the National Institute of Neurological Disorders and Stroke's 'Evaluation of Progression in Multiple Sclerosis by Magnetic Resonance Imaging (MRI)' protocol (NCT00001248). All participants provided informed consent before inclusion. Per this protocol, participants were seen in the clinic and underwent imaging and biospecimen collection. Experienced MS clinicians documented clinical history and determined the Expanded Disability Status Scale (EDSS). We performed Ella assays on the CSF of these participants. These included 21 cases (Supplementary Table 1), all of whom were radiologically and clinically inactive at the time of sample collection. Radiologically and clinically inactive was defined as the absence of any new and/or gadolinium-enhancing lesion(s), and the absence of clinical relapse, respectively, within 6 months of sample acquisition.

In vivo MRI and PRL determination

For the NIH cohort, in vivo MRI acquisition for participants involved using a Siemens Magnetom 7T scanner equipped with a bird-cage-type transmit coil and a 32-channel receive coil. The imaging protocol included a pre-contrast, high resolution three-dimensional gradient dual-echo sequence for acquiring T2*-weighted (T2*) and phase contrast images (a repetition time of 74 ms, echo times of 18, 29.5, 50.0 and 52.4 ms, a flip angle of 10°, an acquisition time of 11 min 50 s per 30 mm slab and 0.5 mm isotropic resolution). Axial T2*-weighted images were motion- and B0-corrected. Magnitude and unwrapped and filtered phase images were also obtained. In addition, a T2-weighted FLAIR sequence was obtained for the visualization of white matter lesions.

The paramagnetic rim lesions (PRLs) were determined by an experienced neuroradiologist on the basis of the NAIMS consensus criteria[69]. To qualify as a PRL, the lesion must be identifiable on T2* or FLAIR and exhibit a discrete paramagnetic rim signal on susceptibility-sensitive sequences including phase. The paramagnetic rim signal should be

continuous through at least two-thirds of the outer edge of the white matter portion of the lesion, and is observed as a hypo-intensity. D.S.R. rated all the PRLs in the NIH cohort.

Ella simple-plex immunoassay of human CSF

The amount of NfL, CXCL13 and BAFF in the CSF collected post mortem from people with MS (Supplementary Table 1) was quantified using Ella simple-plex immunoassay (Bio-Techne), which has been previously validated for the measurement of analytes in MS biofluids[70]. NfL, CXCL13 and BAFF levels were measured using a custom Simple Plex cartridge (Bio-Techne cat. nos. SPCKC-PS- 008065, SPCKB-CS-010515 and ST01B-PS- 002448) on an Ella instrument, according to the manufacturers' instructions. Ella was calibrated using the in-cartridge factory standard curve. All samples were measured in triplicate, with a 1:2 dilution.

Mice

Female 6–10-week-old (young) SJL/J mice were obtained from Envigo and housed at the University of Toronto animal facilities under specific pathogen-free conditions, in a closed caging system with a 12 h light/12 h dark cycle at 21 °C with 50% relative humidity. They were provided with a standard irradiated chow diet (Teklad; Envigo, 2918) and acidified water (reverse osmosis and ultraviolet sterilized). For experiments involving old mice, 6–10-week-old SJL/J mice were purchased and aged at our animal facility until they were 8–12 months old. LTβ$^{-/-}$ mice were originally from B&K Universal and bred in our animal facility. All animal experiments were conducted with ethical approval (protocol number 20011363) from the University of Toronto, Faculty of Medicine Animal Care Committee.

Induction and clinical assessment of EAE

Adoptive transfer EAE in young (6–10 weeks) or old (8–12 months) SJL/J mice was induced as previously described[2]. Briefly, SJL/J donor mice were immunized with 100 µg $PLP_{139–151}$ (HSLGKWLGHPDKF; Canpeptide) in an emulsion of incomplete Freund's adjuvant (BD Difco), supplemented with 200 µg *Mycobacterium tuberculosis* H37 Ra (BD Difco, 231141) in a total volume of 300 µl, administered as three 100 µl subcutaneous injections on the back and flanks. On day 9 after immunization, cells from the spleen and draining lymph nodes (inguinal, cervical, axillary and brachial) were harvested. Lymphocytes were separated using a Percoll gradient and restimulated ex vivo with $PLP_{139–151}$ (10 µg ml^{-1}) in the presence of anti-IFN-γ (20 µg ml^{-1}, Bioceros), anti-IL-4 (20 µg ml^{-1}, Bioceros) and IL-23 (10 ng ml^{-1}, R&D Systems) for 72 h at 37 °C. In total, 1×10^7 cells were injected intraperitoneally into SJL/J recipient mice.

Recipient mice were weighed and scored daily according to a composite scale that we[2,18] and others[71] have previously published. Briefly, the composite scale measures mobility impairments in each limb and the tail. Each limb is graded from 0 (asymptomatic) to 3 (complete paralysis), and the tail is graded from 0 (asymptomatic) to 2 (limp tail). Assessment of the righting reflex is scored from 0 to 2, with 0 being assigned for a normal righting reflex, 1 for slow righting reflex and 2 for a delay of more than 5 s in the righting reflex. Each criterion was measured in 0.5 increments. Thus, the composite score ranges from 0 (nonsymptomatic) to 16 (fully quadriplegic mouse with limp tail and a significantly delayed righting reflex)[71,72].

BTKi and αLTβR or αBAFF treatment

Remibrutinib (LOU064) was synthesized by Novartis. The drug was administered in SJL/J recipient mice twice a day by oral gavage at a dose of 30 mg kg^{-1}, diluted in a sterilized methylcellulose and Tween-80 vehicle (Fujifilm Wako Chemicals and Bioshop, respectively) in an application volume of 10 ml kg^{-1}. For young mice, the drug was administrated from day 3 up to day 11 post-adoptive transfer in the prophylactic modality, or from day 9 up to day 13 post-adoptive transfer in the therapeutic modality. Control mice received the methylcellulose Tween-80 vehicle solution twice a day by oral gavage at the same timepoints after adoptive transfer. For experiments including αLTβR treatment, clone AFH6 (a kind gift from Dr. Ray Jupp, Mestag Therapeutics) and isotype control (αHEL; IgG1 antibody) were administered intraperitoneally on day 8 and day 12 post-adoptive transfer (100 µg per mouse). On days where the αLTβR/αHEL were to be administered along with the BTKi (on day 12 post-adoptive transfer), αLTβR/αHEL was administered first, before vehicle or BTKi treatment. For experiments including αBAFF treatment, an αBAFF antibody (Sandy-2, Adipogen) or mouse IgG1 isotype controls (SouthernBiotech) were delivered intraperitoneally at a dose of 2 mg kg^{-1} on days −2 and 5 relative to the day of the adoptive transfer. For old mice, the drug was administrated from day 9 to day 21 for the histology readout, or from day 9 to day 39 for the MRI readout. Mice were randomized into either the treatment or control groups.

Tissue harvest and processing

For histology/immunohistochemistry and serum NfL measurements at acute and post-acute disease phases, mice were euthanized at the peak phase of disease corresponding to 12–14 days post-adoptive transfer or at the post-acute phase corresponding to 22 or 40 days post-adoptive transfer, depending on the readout. At the time of sacrifice, blood was collected via cardiac puncture and serum was separated and stored at −80 °C until used. Mice were intracardially perfused with 30 ml of PBS. Brains and spinal cords were dissected from the skull and spinal columns. The two brain hemispheres were sagitally divided. One hemisphere was postfixed together with the spinal cord in 10% buffered formalin (MilliporeSigma) for 1 week at 21 °C before being processed in paraffin for pathological analysis. The other hemisphere was postfixed in 10% buffered formalin for 1 h at 21 °C followed by immersion in 30% sucrose overnight at 4 °C, then placed in plastic molds with optimal cutting temperature mounting medium (Thermo Fisher Scientific), frozen in a bath of 2-*O*-methylbutane on dry ice (Fisher Chemical, Thermo Fisher Scientific) and stored at −80 °C until they were sectioned for staining.

To test for the BTK occupancy, a subset of BTKi-treated mice and vehicle-treated mice were euthanized at peak disease and transcardially perfused. Spleen and brains were collected and frozen for later measurements.

BTK occupancy

Meso scale discovery-based sandwich immunoassays for free and total BTK were performed as described in ref. 19. Briefly, for free BTK measurements, samples were incubated with a biotinylated covalent BTK probe, then samples were added to streptavidin ELISA plates to allow binding of probe-bound BTK. The binding of the probe to BTK is mutually exclusive to compound binding to BTK. Plate-bound BTK was detected with an anti-BTK antibody (D3H5, Cell Signaling Technology). For total BTK measurements, an ELISA plate was coated with D3H5 anti-BTK to capture total BTK. An anti-BTK antibody (number 53, BD Biosciences) directed to a different epitope was then used to detect captured BTK. The respective free BTK levels for each sample were normalized to the total BTK level in the same sample, and these ratios were expressed as percentages of the vehicle control samples.

Preparation of samples for MRI

Mice destined for MRI were sacrificed by CO_2 asphyxiation and transcardially perfused using a peristaltic pump at a rate of 1 ml min^{-1}. Mice were first perfused with 40 ml of PBS containing 2 mM ProHance (Bracco Diagnostics) and 400 USP heparin (Fresnius Kabi), followed by 30 ml of PBS containing 2 mM ProHance and 4% paraformaldehyde (EMS). Mice were decapitated, and skulls were placed into PBS containing 2 mM ProHance and 4% paraformaldehyde (EMS). After an overnight incubation at 4 °C, skulls were transferred to PBS containing 2 mM ProHance with 0.02% sodium azide (Fisher Scientific). Following a 30-day-incubation, skulls were scanned by MRI at the Mouse Imaging Centre in the Centre for Phenogenomics in Toronto, Ontario, Canada.

Anatomical image acquisition

A 7-tesla 306-mm horizontal-bore magnet (BioSpec 70/30 USR, Bruker) with a ParaVision 6.0.1 console[73] was used to image brains in skulls. Four to eight samples were imaged in parallel using a custom-built eight-coil solenoid array. Anatomical image acquisition was modeled from ref. 74 with the following scan parameters: T2W three-dimensional FSE cylindrical *k*-space acquisition sequence, repetition time, echo time and echo train length (ETL) of 350 ms, 12 ms and 6, respectively, effective echo time (TEeff) of 30 ms, 4 effective averages, a field of view (FOV)/matrix size of 20.2 × 20.2 × 25.2 mm/504 × 504 × 630, and total imaging time of 13.2 h. The resulting anatomical images had an isotropic resolution of 40 µm voxels.

MRI registration and analysis

To assess any changes to the mouse brains owing to age and treatment, all anatomical brain images were registered together using the mni_autoreg[75] and Advanced Normalizations Tools[76] tool kits. The resulting consensus average and Jacobian determinants were used to quantify volumetric differences between each MRI image and the average. The MAGeT pipeline[77] was used to segment images using a 3D brain atlas.

Simoa assay for serum NfL

The amount of NfL in mouse serum was quantified with a single-molecule array (Simoa) NF-light assay (Quanterix). In brief, magnetic beads were conjugated with monoclonal capture antibodies (mAB47:3, UmanDiagnostics), then incubated with diluted mouse serum (1:8 or 1:16 dilution) and biotinylated detection antibodies (mAB2:1, UmanDiagnostics). Upon adding streptavidin-conjugated β-galactosidase (Quanterix), Resorufin β-D-galactopyranoside (Quanterix) was added for detection. The experiment was performed on a Simoa HD-X Analyzer (Quanterix). The assay was performed in duplicates, and the mean of the two measured serum NfL values per sample is reported.

scRNAseq

Data from our previously published leptomeninges single-cell dataset (GSE201568)[17] was loaded into RStudio (v2023.03.0) and analyzed using the Seurat package (v5.1.0)[21]. After quality control, data scaling and normalization, an unsupervised clustering of 16,568 cells was performed, resulting in identification of eleven unique cell clusters. Using canonical lineage markers, we were able to identify B cells (*Ms4a1*, *Cd19*, *Ighm* and *Ighd*), $Cd8^+$ T cells (*Cd3* and *Cd8a*), $Cd4^+$ Th1 cells (*Cd3e*, *Cd4* and *Tbx21*), $Cd4^+$ Th17 cells (*Cd3e*, *Cd4*, *Rorc* and *Il17a*), neutrophils (*Cxcr2*, *Ly6g* and *Itgam*), $Ly6c^+$ myeloid cells (*Itgam*, *Ly6c2*, *Csf1r* and *Aif1*), microglia/macrophages (*Itgam*, *Aif1*, *Hexb*, *Tmem119* and *P2ry12*), dendritic cells (DCs) (*Itgax*, *Flt3* and *Ccr7*), stromal cells (*Col1a1*, *Pdgfra*, *Fn1* and *Pdpn*) and endothelial cells (*Pecam1* and *Cd34*). Visualization of gene expression and co-expression in individual clusters was performed using the VlnPlot and FeaturePlot functions.

Dissection of the leptomeninges for T cell stimulation and flow cytometry

Under a dissection microscope, leptomeninges were removed from the brainstem, cerebellum, ventricles, hypothalamus and cortex into a digestion buffer (RPMI 1640 with 10 mM HEPES, 1% penicillin–streptomycin, 1% GlutaMAX and 2% fetal bovine serum (FBS), pH 7.4) containing DNAse I (60 µg ml^{-1}) and collagenase P (1 mg ml^{-1}). Collected cells from leptomeninges were washed twice in ice-cold PBS and resuspended in complete RPMI (10% FBS, Thermo Fisher Scientific; L-glutamine, MilliporeSigma; sodium pyruvate, MilliporeSigma; penicillin, MilliporeSigma; streptomycin, MilliporeSigma; HEPES pH 7.0, Thermo Fisher Scientific; and β-mercaptoethanol, Thermo Fisher Scientific, in RPMI 1640 medium, MilliporeSigma). Cells were counted with a hemocytometer and incubated at 37 °C for 5 h with an intracellular cytokine re-stimulation buffer (PMA, MilliporeSigma; stock 500 µg ml^{-1}) used at 1:100,000, ionomycin (MilliporeSigma; stock 0.5 mg ml^{-1}) used at 1:1,000 and Brefeldin A (Thermo Fisher Scientific, stock 100×) used at 1:1,000 in complete RPMI. At the end of the incubation, cells were collected, washed twice in ice-cold PBS and resuspended in PBS with 2% FBS and stained with Live/Dead Fixable Aqua (Life Technologies, Thermo Fisher Scientific) at 1:1,000 in PBS for 30 min at 4 °C, followed by staining with anti–CD4 (mAb, RM4-5) and anti-CD3 (mAb, 17A2) in PBS with 2% FBS and 1 mg ml^{-1} Fc block. Cells were then permeabilized with CytoFix/CytoPerm (BD Biosciences) for 20 min at 4 °C, then stained with anti-GM-CSF-FITC (mAb, MP1-22E9), anti-IL-17A (mAb, 17B7) and anti-IFN-γ (mAb, XMG1.2) in 1× Perm/Wash buffer with 1 mg ml^{-1} Fc block (Supplementary Table 2). Cells were acquired by FACS using the BD LSR X-20 II instrument and FACSDiva software (BD Biosciences). Data analysis was done with FlowJo v10.5.3 software.

In vitro culture of splenocytes and LTβ staining by flow cytometry

SJL/J and $LT\beta^{-/-}$ mice were euthanized by CO_2 asphyxiation and spleens were collected and mashed through 70-µm filters into culture medium (RPMI 1640, Sigma-Aldrich) supplemented with 10% FBS (Gibco), 1× penicillin:streptomycin (Sigma-Aldrich) and 1× L-Glutamie (Sigma-Aldrich). Splenocytes were resuspended in 5 ml of RBC lysis buffer (eBioscience, 00-4333-57) for 5 min to remove red blood cells. Cells were washed and resuspended in culture media at 2×10^6 ml^{-1}. Then, 200 ul of cell suspension per well was plated in 96-well U-bottomed culture plates. Cells were placed in the incubator at 37 °C 5% CO_2 for 1 h to rest, then BTKi (or culture medium) was added at a concentration of 10 nM for 1 h. InVivoMAb anti-mouse CD40 (BioxCell, BE0016-2; 5 µg ml^{-1}) + LPS (Sigma-Aldrich L2880; 1 µg ml^{-1}) were added to the culture overnight (18–20 h). Cells were harvested, washed with PBS and stained with Live/Dead Fixable Aqua (Invitrogen) at a dilution of 1:1,000 for 20 min on ice. Surface markers were stained in 2% FBS in PBS for 30 min on ice (Supplementary Table 2). Samples were acquired on a BD FACSymphony A3 using the FACSDiva software. Flow cytometry data were analyzed using FlowJo v10.0.

qPCR on leptomeninges

Leptomeninges were collected in digestion buffer (RPMI 1640 with 10 mM HEPES, 1% penicillin–streptomycin, 1% GlutaMAX and 2% FBS, pH 7.4) containing DNAse I (60 µg ml^{-1}) and collagenase P (1 mg ml^{-1}). RNA was extracted with Qiagen RNeasy Microkit (Qiagen, 74004). RNA concentration and quality were assessed by NanoDrop. cDNA synthesis was performed using Invitrogen SuperScript IV First-Strand Synthesis System, and cDNA was subjected to qPCR reactions with Rpl19 as an internal control using the following primers: LTα forward primer AGCCCATCCACTCCCTCAGAAG and reverse primer TGCTCTCCAGAGCAGTGAGTTC and LTβ forward primer CCTGTTGTTGGCAGTGCCTATC and reverse primer GACGGTTTGCTGTCATCCAGTC (Integrated DNA Technologies).

Statistics

All statistical tests were run using GraphPad Prism (version 10.2.1). All quantification data were subjected to Shapiro–Wilk normality tests for equality of variances. Only *P* values less than 0.05 were considered significant. The statistical tests used for each experimental dataset are indicated in the figure captions. All murine experiments were performed at least three times with reproducible results. In all plots, each dot represents a measurement from a distinct sample. No statistical methods were used to predetermine sample sizes, but our sample sizes are similar to those reported in our previous publications[17,18,27,34].

Reporting summary

Further information on research design is available in the Nature Portfolio Reporting Summary linked to this article.

Data availability

All data supporting the findings of this study are available within the paper and its Extended Data Information. Source data are provided with this paper.

References

66. Luchetti, S. et al. Progressive multiple sclerosis patients show substantial lesion activity that correlates with clinical disease severity and sex: a retrospective autopsy cohort analysis. *Acta Neuropathol.* **135**, 511–528 (2018).
67. Frischer, J. M. et al. The relation between inflammation and neurodegeneration in multiple sclerosis brains. *Brain* **132**, 1175–1189 (2009).
68. Michailidou, I. et al. Complement C1q–C3-associated synaptic changes in multiple sclerosis hippocampus. *Ann. Neurol.* **77**, 1007–1026 (2015).
69. Bagnato, F. et al. Imaging chronic active lesions in multiple sclerosis: a consensus statement. *Brain* **147**, 2913–2933 (2024).
70. Gauthier, A. et al. Comparison of Simoa and Ella to assess serum neurofilament-light chain in multiple sclerosis. *Ann. Clin. Transl. Neurol.* **8**, 1141–1150 (2021).
71. Giuliani, F., Fu, S. A., Metz, L. M. & Yong, V. W. Effective combination of minocycline and interferon-beta in a model of multiple sclerosis. *J. Neuroimmunol.* **165**, 83–91 (2005).
72. Galicia, G. et al. Isotype-switched autoantibodies are necessary to facilitate central nervous system autoimmune disease in *Aicda*$^{-/-}$ and *Ung*$^{-/-}$ mice. *J. Immunol.* **201**, 1119–1130 (2018).
73. Arbabi, A. et al. Multiple-mouse magnetic resonance imaging with cryogenic radiofrequency probes for evaluation of brain development. *NeuroImage* **252**, 119008 (2022).
74. Spencer Noakes, T. L., Henkelman, R. M. & Nieman, B. J. Partitioning *k*-space for cylindrical three-dimensional rapid acquisition with relaxation enhancement imaging in the mouse brain. *NMR Biomed.* https://doi.org/10.1002/nbm.3802 (2017).
75. Collins, D. L., Neelin, P., Peters, T. M. & Evans, A. C. Automatic 3D intersubject registration of MR volumetric data in standardized Talairach space. *J. Comput. Assist. Tomogr.* **18**, 192–205 (1994).
76. Avants, B. B. et al. A reproducible evaluation of ANTs similarity metric performance in brain image registration. *NeuroImage* **54**, 2033–2044 (2011).
77. Chakravarty, M. M. et al. Performing label-fusion-based segmentation using multiple automatically generated templates. *Hum. Brain Mapp.* **34**, 2635–2654 (2013).

Acknowledgements

This work was supported by the National Multiple Sclerosis Society grant no. RFA-2203-39259 to J.L.G. and V.R., by the MS Canada grant no. 1423841 to J.L.G., by the CIHR (Aging Research Program) grant no. 525895, by Office of the Assistant Secretary of Defense for Health Affairs through the (Multiple Sclerosis Research Program) under award no. HT9425-23-1-0933 to J.L.G. and V.R., and by the Canada Research Chair in Tissue Specific Immunity to J.L.G. Opinions, interpretations, conclusions and recommendations presented in this paper are those of the authors and are not necessarily endorsed by the Department of Defense. This research was supported in part by the Intramural Research Program of the National Institute of Neurological Disorders and Stroke of the National Institutes of Health (ZIA NS003119, D.S.R.). The contributions of the NIH authors are considered Works of the US Government. The findings and conclusions presented in this paper are those of the authors and do not necessarily reflect the views of the NIH or the US Department of Health and Human Services. We thank R. Jupp from Mestag Therapeutics for providing the αLTβR agonist.

Author contributions

I.N., V.R., M.Z., K.C.-J., A.W., A. Pangan, A. Pu and L.W. contributed to the induction and monitoring of the EAE experiments. I.N., V.R., A. Pangan, J.P. and F.N.S. performed the immunostaining and analyses of the mouse brain tissues. J.S.Y.A. performed the dissection and the qPCR analysis of the leptomeninges in the animal studies. B.C. and B.N.-H. advised on the experiments and performed the BTKi occupancy assays. A.-K.P. and E.P. performed the quantification and analyses of serum NfL in the animal studies. S.S. and J.G.S. performed the mouse MRI measurements. V.R. and J.Z. performed the quantification and analysis of the CSF NfL, GFAP, BAFF and CXCL13 in the post mortem MS cohort. S.A.R. and D.S.R. performed the quantification and analysis of the CSF NfL, GFAP, BAFF and CXCL13 in the living MS cohort. J.L.B. advised of LT biology. J.L.G. and V.R. designed the study and wrote the paper.

Competing interests

J.L.G. has a shared patent on 'Methods of treating an autoimmune disease': WO2020102895A1, US20210401939A1, EP3883593A4 and CA3120454A1. The patent provides methods of treating an autoimmune disease (for example, multiple sclerosis) or reducing inflammation by administering at least a B cell activating Factor (BAFF) polypeptide to a subject in need thereof. The effect of BAFF on plasmablast/plasma cells and their role in autoimmune diseases is also disclosed. D.S.R. has received research funding from Abata and Sanofi, related to but separate from his contribution to the current work. The other authors declare no competing interests. B.C. and B.N.-H. are employees of Novartis.

Additional information

Extended data is available for this paper at https://doi.org/10.1038/s41590-025-02359-5.

Supplementary information The online version contains supplementary material available at https://doi.org/10.1038/s41590-025-02359-5.

Correspondence and requests for materials should be addressed to Jennifer L. Gommerman or Valeria Ramaglia.

Peer review information *Nature Immunology* thanks David Hafler and the other anonymous reviewer(s) for their contribution to the peer review of this work. Peer reviewer reports are available. Primary Handling Editor: L.A. Dempsey, in collaboration with the *Nature Immunology* team.

https://doi.org/10.1038/s41590-025-02359-5

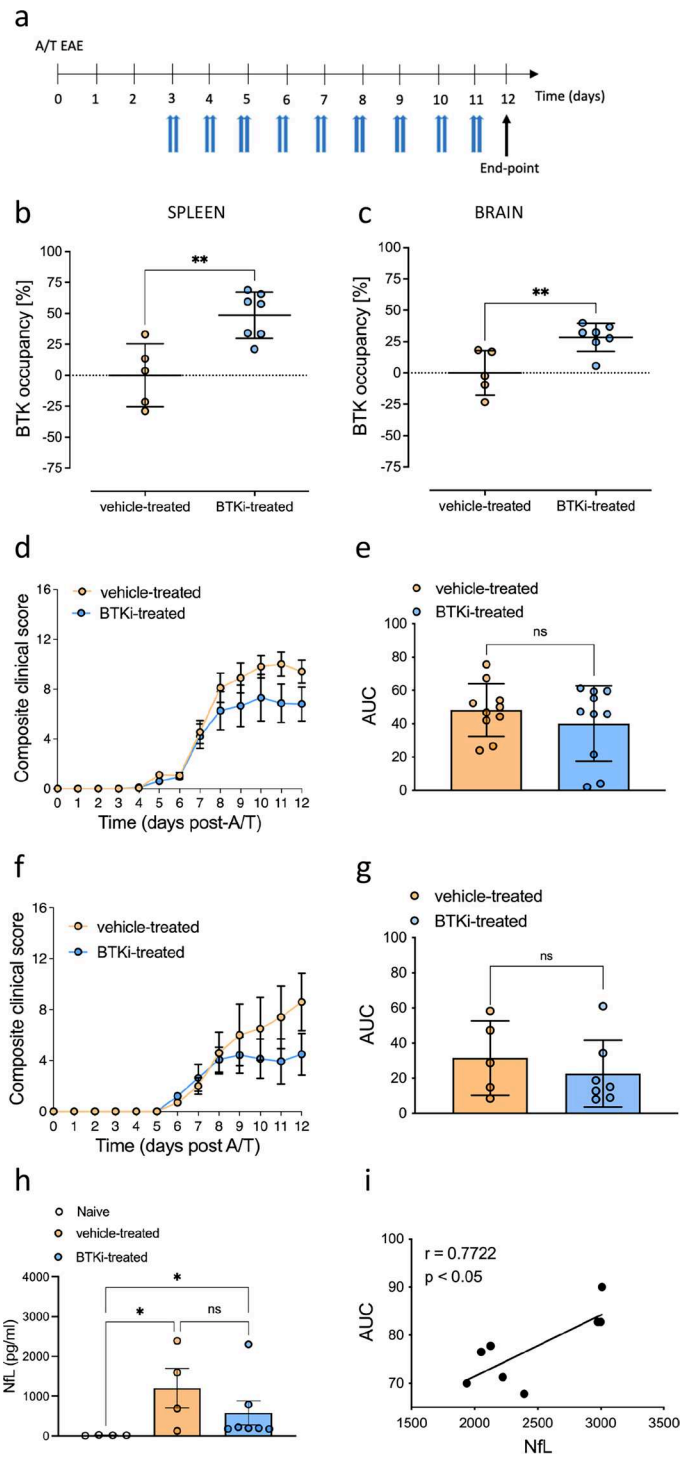

Extended Data Fig. 1 | Prophylactic BTK inhibition does not affect clinical outcome or serum neurofilament light (NfL) levels in SJL/J adoptive transfer EAE mice. (**a**) Female 6- to 10-week-old SJL/J mice received an adoptive transfer of 10 million encephalitogenic T_H17 cells to induce EAE. Mice were treated via oral gavage with 30 mg/kg Bruton's tyrosine kinase inhibitor (BTKi, Remibrutinib, (LOU064) or vehicle control twice a day prophylactically from day 3 to day 11 after adoptive transfer and were harvested at peak EAE (day 12 after adoptive transfer). (**b**, **c**) BTK occupancy in the spleen and brain of vehicle-treated ($n = 5$ for each) or BTKi-treated ($n = 7$ for each) SJL/J adoptive transfer EAE mice at peak disease. (**d**–**g**) Clinical scores and area under the curves (AUC) of the clinical scores in 2 experiments where SJL/J adoptive transfer EAE mice were treated with the BTK inhibitor ($n = 10$ and n = 7) or vehicle control ($n = 10$ and n = 6) prophylactically. (**h**) Serum neurofilament light chain (NfL) in naïve ($n = 4$), vehicle-treated ($n = 4$) and BTKi-treated ($n = 7$) mice at peak disease. (**i**) Correlation between the AUC and the amount of serum NfL in vehicle–treated or BTKi–treated (n = 8) SJL/J adoptive transfer EAE mice at peak disease. Data are shown as means ± SD. Statistical analysis in **b**, **c**, **e**, **g** was conducted using a two-sided Mann–Whitney test. Statistical analysis in H was conducted using a two-sided Kruskal–Wallis test with post hoc Dunn's multiple comparisons test. Statistical analysis in **d**, **f** was conducted using a One-Way ANOVA test with post hoc Bonferroni multiple comparisons test. Correlation analysis in i was conducted using two-sided Pearson correlation coefficient. $^*P \leq 0.05$ and $^{**}P \leq 0.01$. (b):p = 0.002, (**c**):p = 0.0051, (**h**): naïve vs vehicle-treated p = 0.0216 and naïve vs BTKi-treated p = 0.0403.

https://doi.org/10.1038/s41590-025-02359-5

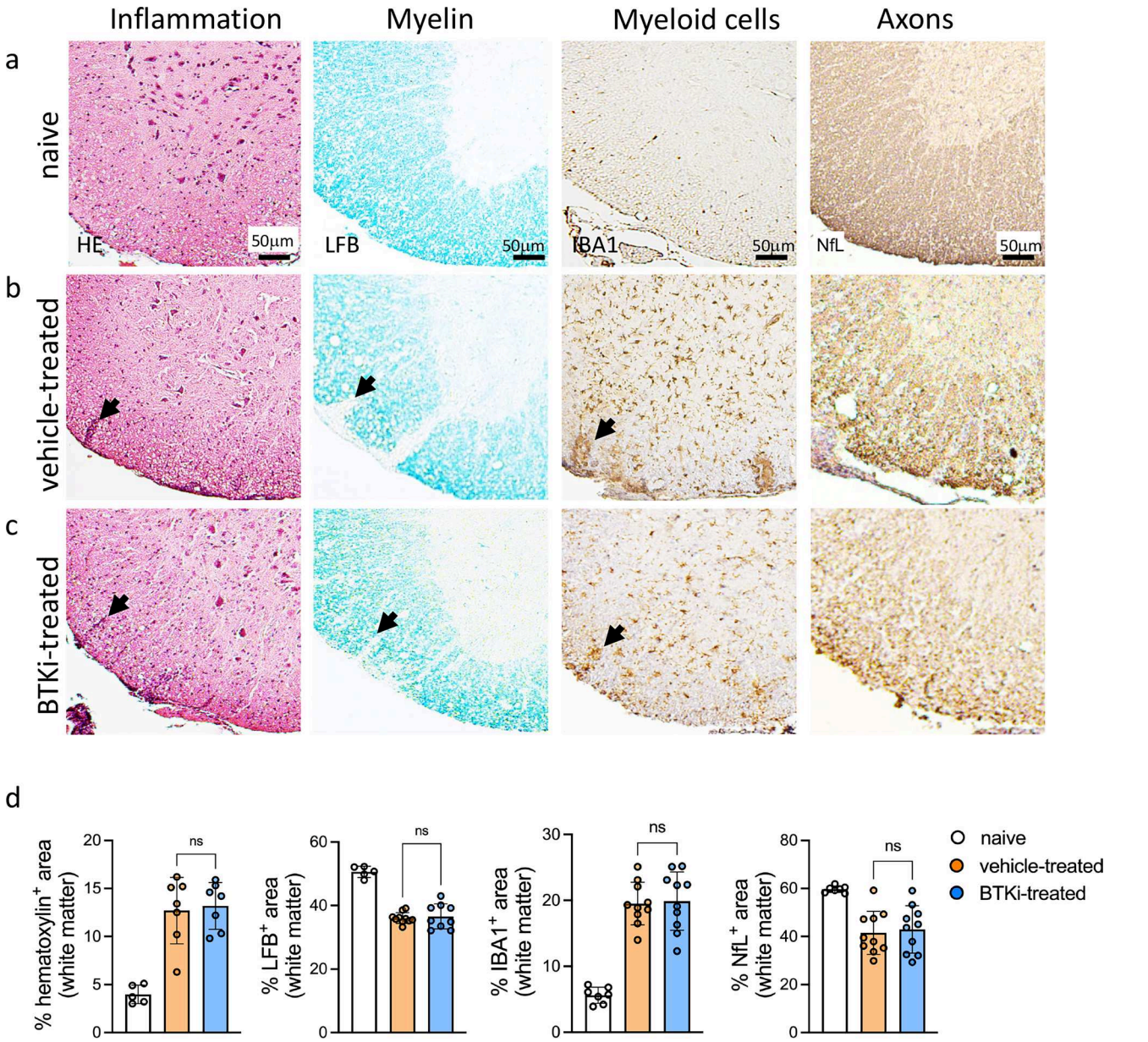

Extended Data Fig. 2 | Prophylactic BTK inhibition does not affect spinal cord pathology in SJL/J adoptive transfer EAE mice. Histology and immunohistochemical staining of spinal cord tissue from naïve (**a**), prophylactically vehicle–treated (**b**) and BTK inhibitor (BTKi)–treated (**c**) SJL/J adoptive transfer EAE mice at peak disease (day 12 after adoptive transfer) for H&E visualizing inflammation, luxol fast blue (LFB) visualizing myelin, ionized calcium binding adapter molecule 1 (IBA1) visualizing microglia and macrophages and neurofilament light chain (NfL) visualizing axons. Black arrowheads indicate the inflamed and damaged spinal cord white matter area. (**d**) Quantification of **a**-**c**. Data are shown as means ± SD. Statistical analysis was conducted using Kruskal–Wallis tests with post hoc Dunn's multiple comparisons test. $P > 0.05$. (naïve: n = 5, 5, 7 and 7 respectively), (vehicle-treated: n = 10 for each graph), (BTKi–treated: n = 10 for each graph).

https://doi.org/10.1038/s41590-025-02359-5

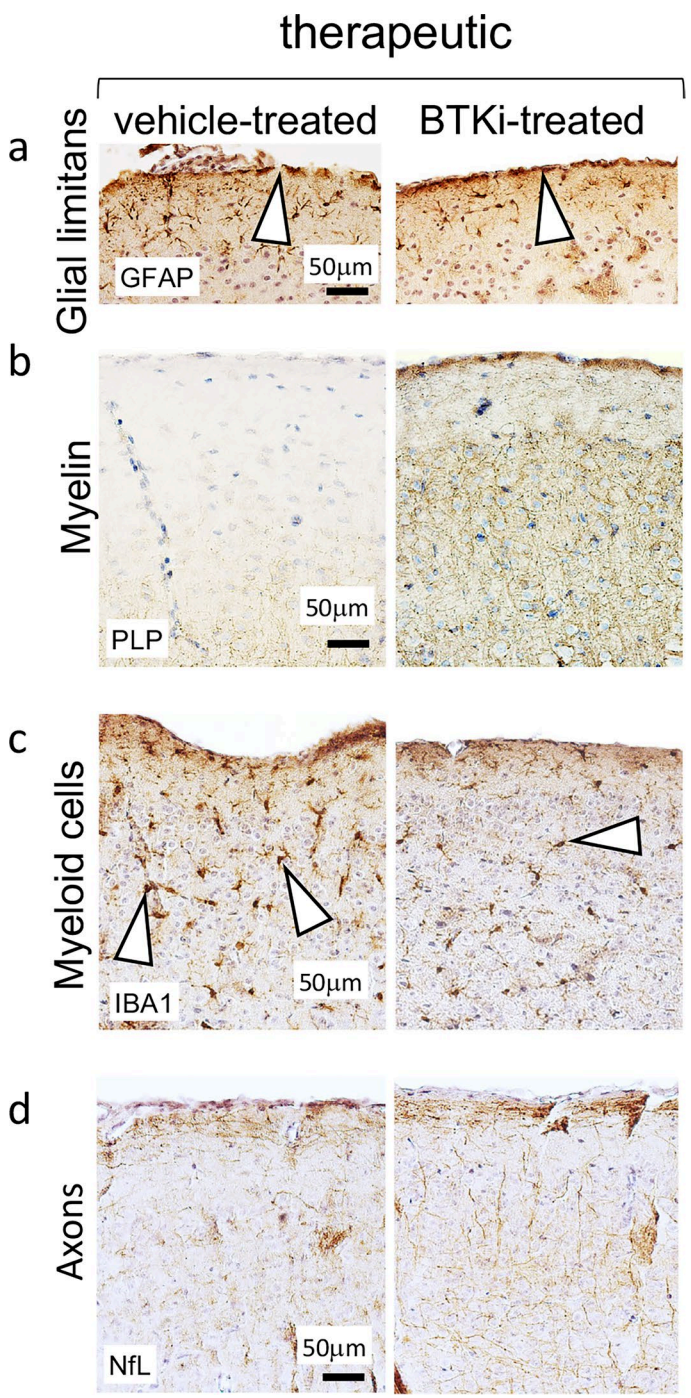

Extended Data Fig. 3 | Therapeutic BTK inhibition spares the glial limitans, reduces cortical gray matter demyelination, myeloid cell accumulation and axonal loss in SJL/J adoptive transfer EAE. Immunohistochemical staining of somatosensory cortex tissue from naïve, therapeutically vehicle–treated and BTK inhibitor (BTKi)–treated SJL/J adoptive transfer EAE mice at peak disease (day 12 after adoptive transfer) for glial fibrillary acidic protein (GFAP) visualizing the glial limitans (**a**), proteolipid protein (PLP) visualizing myelin (**b**), ionized calcium binding adapter molecule 1 (IBA1) visualizing microglia and macrophages (**c**) and neurofilament light chain (NfL) visualizing axons (**d**). White arrowheads in a indicate the glial limitans; in c indicate microglia/macrophages.

https://doi.org/10.1038/s41590-025-02359-5

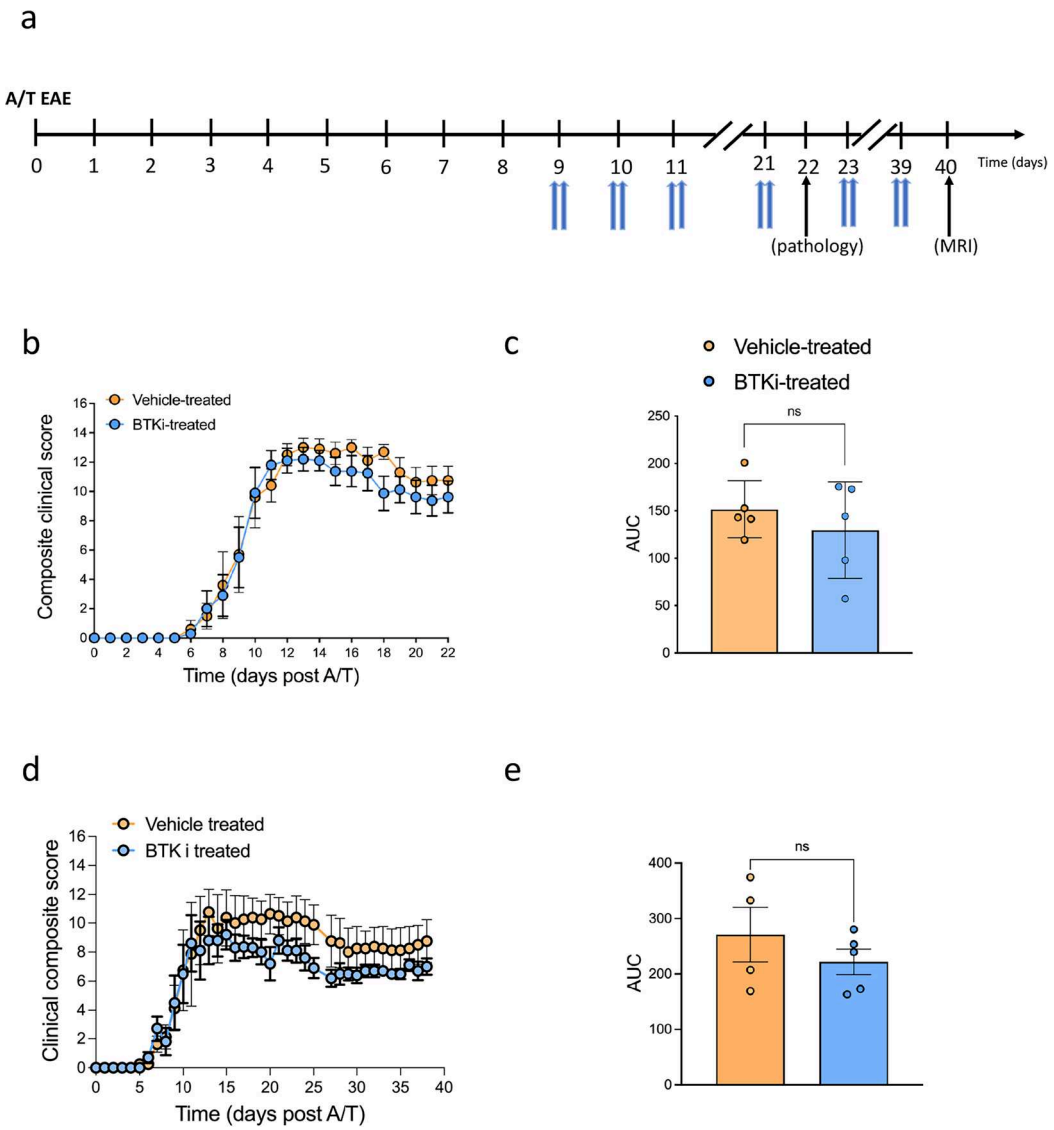

Extended Data Fig. 4 | Therapeutic BTK inhibition does not affect clinical outcome in old SJL/J adoptive transfer EAE mice. a) Female 8 to 12 moths-old SJL/J mice received an adoptive transfer of 10 million encephalitogenic T_H17 cells to induce EAE. Mice were treated via oral gavage with 30 mg/kg Bruton's tyrosine kinase inhibitor (BTKi, Remibrutinib, LOU064) or vehicle control twice a day therapeutically from day 9 to day 21 post-adoptive transfer (**b**, **c**) when the tissue was harvested for pathology assessment or day 39 post-adoptive transfer (**d**, **e**) when the tissue was harvested for MRI assessment. Timeline and area under the curves (AUC) of the clinical scores from the pathology (**b**, **c**; *n* = 5 for BTKi treated and *n* = 5 for vehicle treated mice) and the MRI (**d**, **e**; *n* = 7 for BTKi treated and n = 7 for vehicle treated mice) experiments. Data are shown as means ± SD. Statistical analysis in B and D was conducted using a two-sided One-Way ANOVA test with post hoc Bonferroni multiple comparisons test. Statistical analysis in C and E was conducted using a two-sided Mann–Whitney test.

https://doi.org/10.1038/s41590-025-02359-5

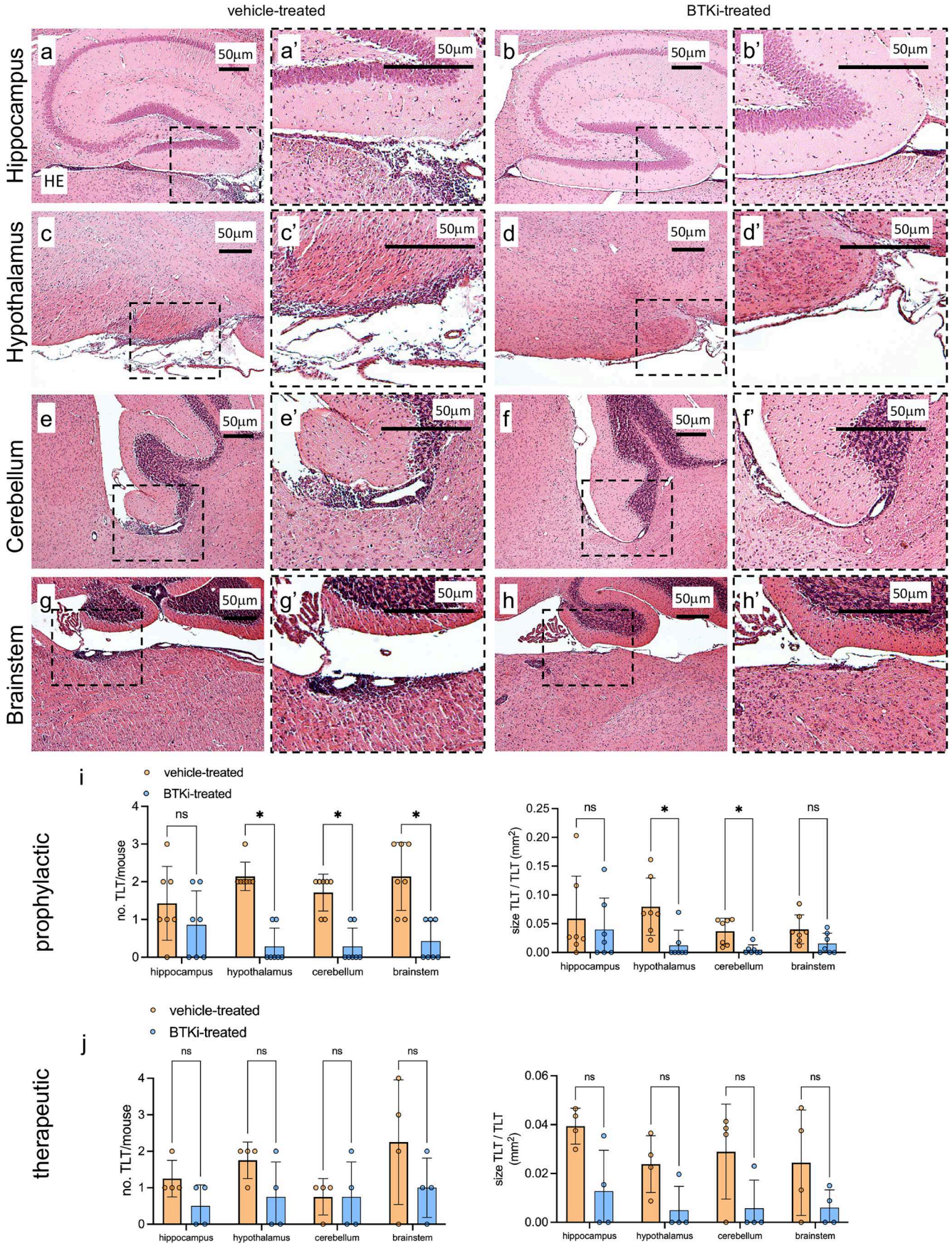

Extended Data Fig. 5 | See next page for caption.

https://doi.org/10.1038/s41590-025-02359-5

Extended Data Fig. 5 | Effects of prophylactic or therapeutic BTK inhibition on leptomeningeal TLTs in SJL/J adoptive transfer EAE mice. Representative hematoxylin & Eosin (H&E)–stained sections of the leptomeninges overlaying the hippocampi (**a**, **b**), hypothalami (**c**, **d**), cerebelli (**e**, **f**) and brainstems (**g**, **h**) of vehicle–treated or BTK inhibitor (BTKi)–treated SJL/J adoptive transfer EAE mice at peak disease (day 12 after adoptive transfer). Quantification of the number and size of leptomeningeal TLTs shown in A-H for the prophylactic (**i**) or therapeutic (**j**) treatment modality. Data are shown as means ± SD. Statistical analysis was conducted using two-sided multiple Mann–Whitney tests. ns, not significant; $^{*}P \leq 0.05$. (vehicle-treated: n = 7 for each treatment modality), (BTKi–treated: n = 7 for each treatment modality).

https://doi.org/10.1038/s41590-025-02359-5

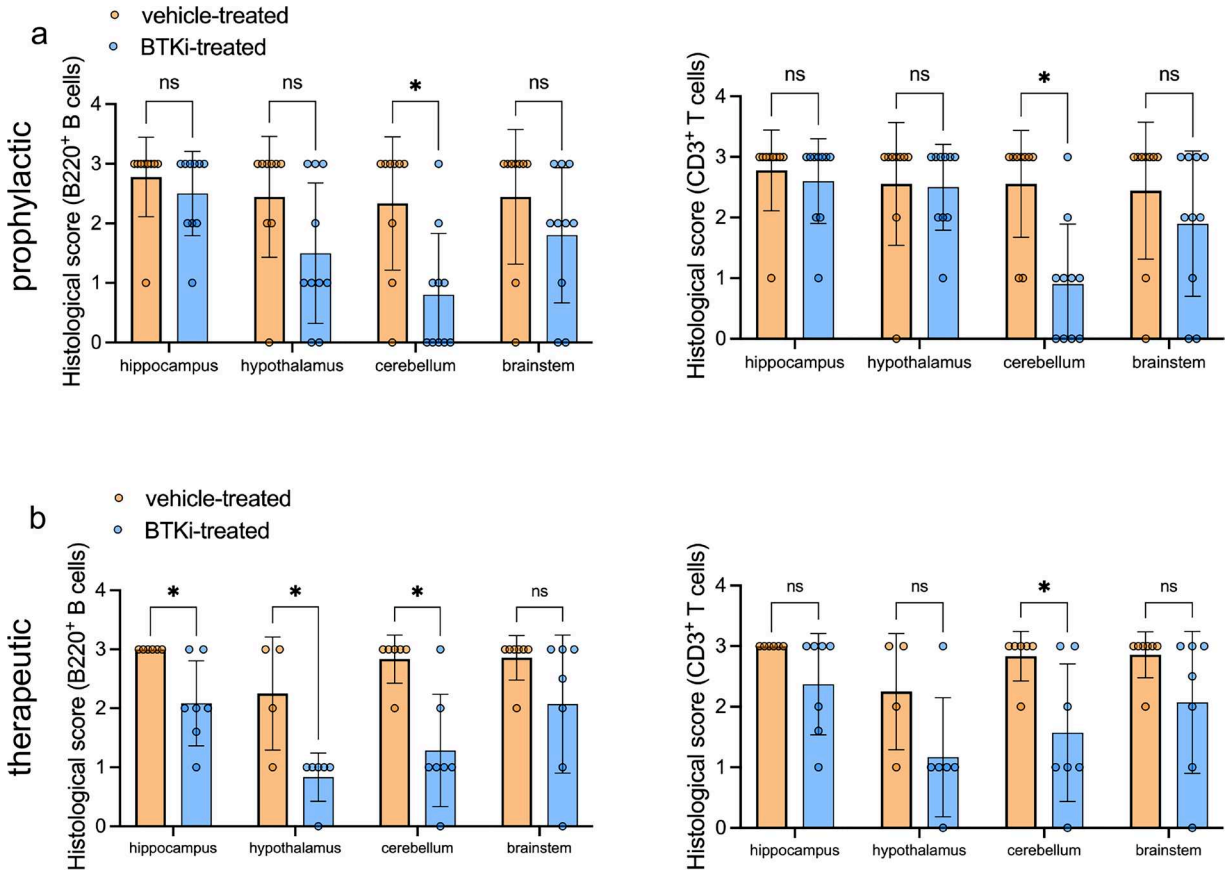

Extended Data Fig. 6 | Effects of prophylactic or therapeutic BTK inhibition on leptomeningeal B and T cells in SJL/J adoptive transfer EAE mice. Histological score of B220$^+$ B cells and CD3$^+$ T cells in the leptomeninges of prophylactically (**a**) or therapeutically (**b**) vehicle–treated or BTK inhibitor (BTKi)–treated SJL/J adoptive transfer EAE mice at peak disease (day 12 after adoptive transfer). Data are shown as means ± SD Statistical analysis was conducted using multiple Mann–Whitney tests. ns, not significant; *$P \leq 0.05$. (**a**) B220, p = 0.011994; CD3, p = 0.003767. (**b**) B220, hippocampus p = 0.020979; hypothalamus p = 0.028571; cerebellum p = 0.011072. CD3, cerebellum p = 0.049534. $n = 7$ (vehicle-treated), 7 (BTKi–treated).

https://doi.org/10.1038/s41590-025-02359-5

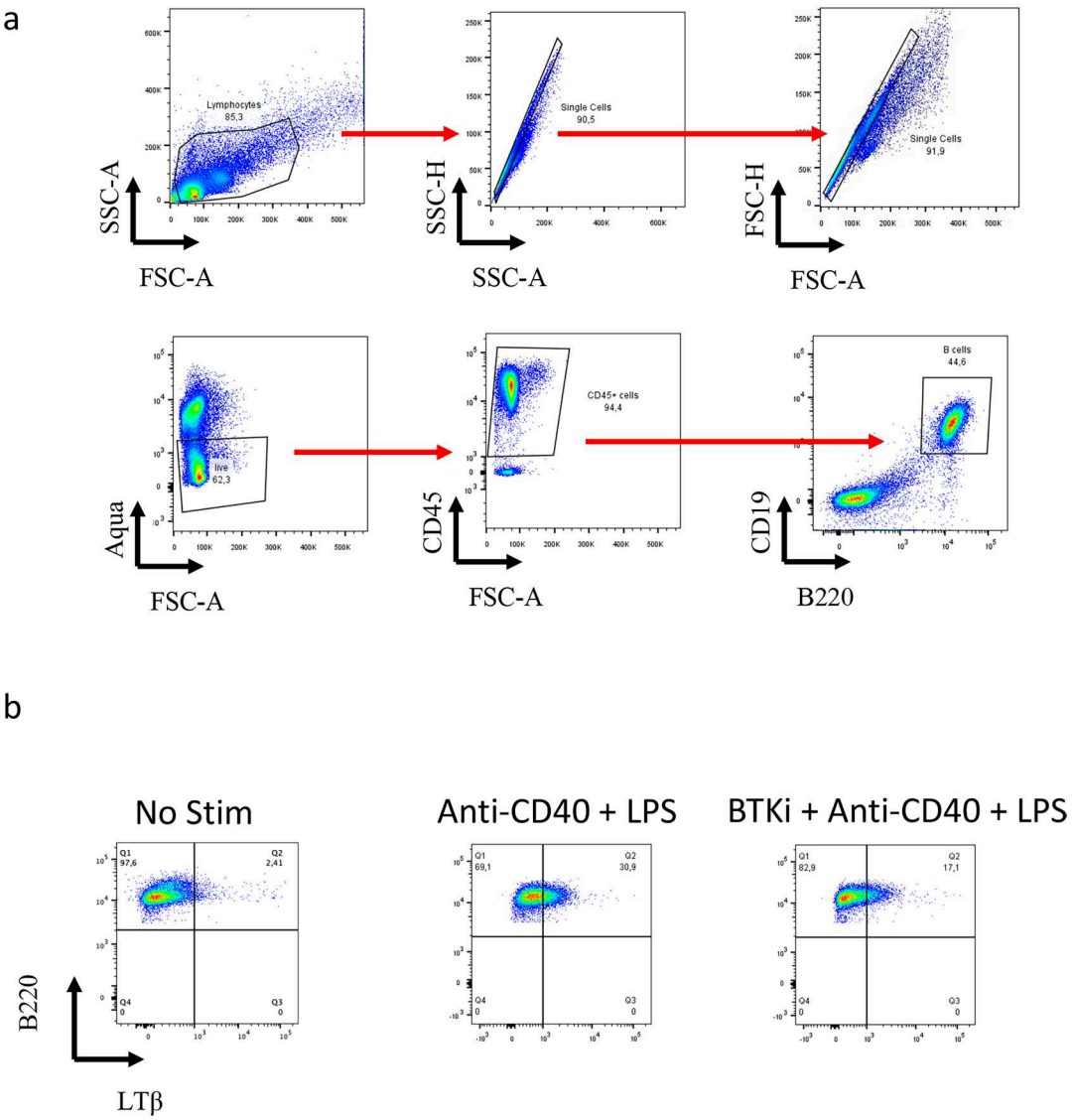

Extended Data Fig. 7 | Gating strategy for B cells treated with BTKi. a) Gating strategy for B cells. (**b**) Representative plots of LTβ^{+}CD19^{+}B220^{+} B cells from naive SJL/J splenocytes either unstimulated or stimulated with mouse anti-CD40 (5ug/ml) + LPS (1ug/ml) *ex vivo* after pre-treatment with BTKi (10 nM) or equivalent Vol of culture medium for 1 h.

https://doi.org/10.1038/s41590-025-02359-5

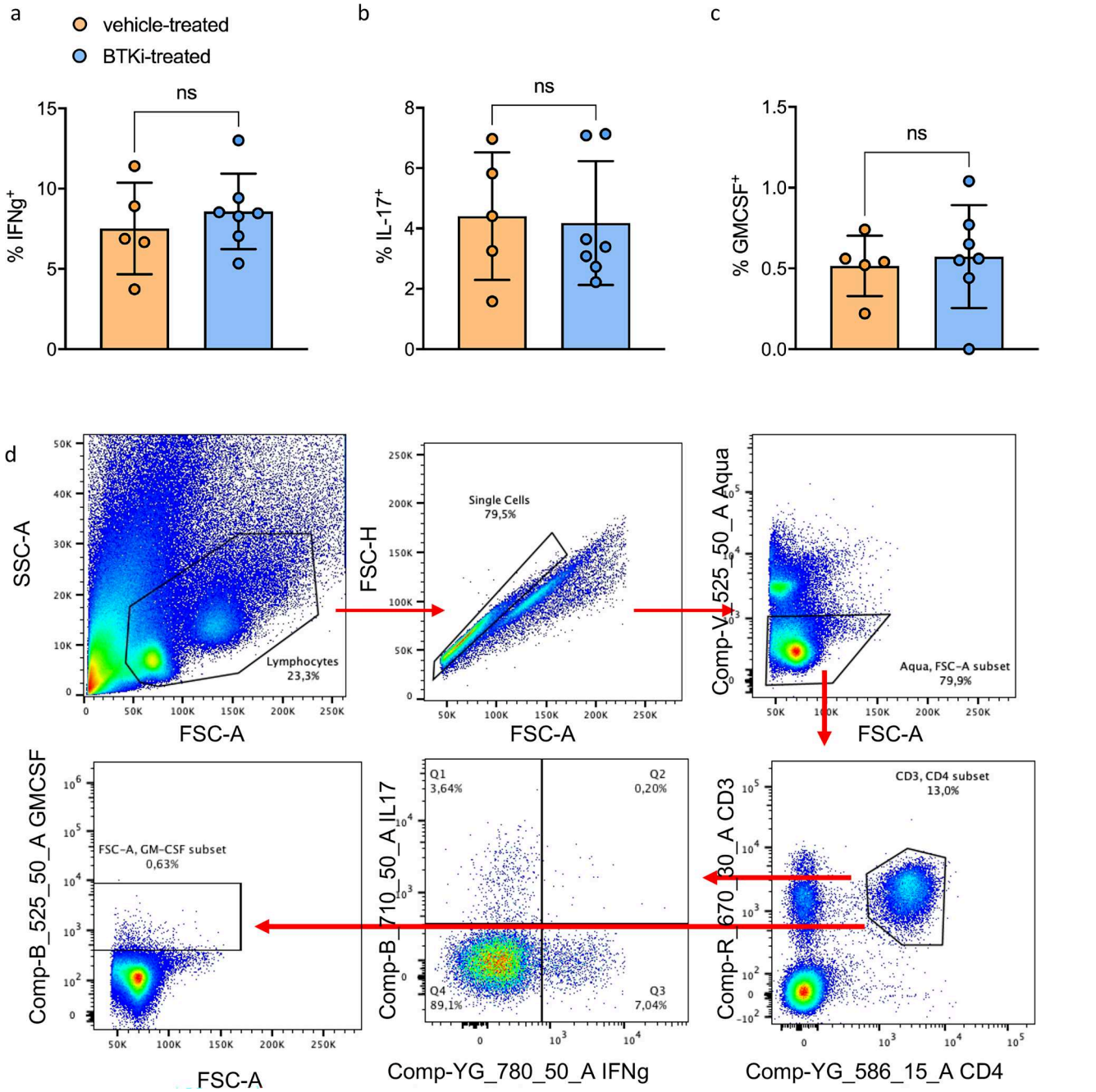

Extended Data Fig. 8 | Prophylactic BTK inhibition does not impact the pro-inflammatory profile of T cells in the leptomeninges of SJL/J adoptive transfer EAE mice. Flow cytometry quantification of interferon (IFN)-γ (**a**), interleukin (IL)-17A (**b**) and granulocyte-macrophage colony-stimulating factor (GM-CSF) (**c**) production by $CD3^+CD4^+$ T cells from single cell suspensions isolated from the leptomeninges and stimulated for 4 h in 1X Cell Stimulation Cocktail with 1X Brefeldin A. (**d**) Gating strategy of **a**-**c**. Data are shown as means ± SD.Statistical analysis was conducted using a two-sided Mann–Whitney test. ns, not significant. $n = 5$ (vehicle-treated), 7 (BTKi–treated).

nature portfolio

Corresponding author(s): Jennifer Gommerman and Valeria Ramaglia

Last updated by author(s): Oct 25, 2025

Reporting Summary

Nature Portfolio wishes to improve the reproducibility of the work that we publish. This form provides structure for consistency and transparency in reporting. For further information on Nature Portfolio policies, see our Editorial Policies and the Editorial Policy Checklist.

Statistics

For all statistical analyses, confirm that the following items are present in the figure legend, table legend, main text, or Methods section.

n/a	Confirmed
☐	☒ The exact sample size (*n*) for each experimental group/condition, given as a discrete number and unit of measurement
☐	☒ A statement on whether measurements were taken from distinct samples or whether the same sample was measured repeatedly
☐	☒ The statistical test(s) used AND whether they are one- or two-sided *Only common tests should be described solely by name; describe more complex techniques in the Methods section.*
☐	☒ A description of all covariates tested
☐	☒ A description of any assumptions or corrections, such as tests of normality and adjustment for multiple comparisons
☐	☒ A full description of the statistical parameters including central tendency (e.g. means) or other basic estimates (e.g. regression coefficient) AND variation (e.g. standard deviation) or associated estimates of uncertainty (e.g. confidence intervals)
☐	☒ For null hypothesis testing, the test statistic (e.g. *F*, *t*, *r*) with confidence intervals, effect sizes, degrees of freedom and *P* value noted *Give P values as exact values whenever suitable.*
☒	☐ For Bayesian analysis, information on the choice of priors and Markov chain Monte Carlo settings
☒	☐ For hierarchical and complex designs, identification of the appropriate level for tests and full reporting of outcomes
☐	☒ Estimates of effect sizes (e.g. Cohen's *d*, Pearson's *r*), indicating how they were calculated

Our web collection on statistics for biologists contains articles on many of the points above.

Software and code

Policy information about availability of computer code

Data collection	No software was used
Data analysis	Open source Image processing software ImageJ2, version 2.14.0/1.54f. Zen pro 2.0 imaging software (Zeiss). FlowJo version 10.10.GraphPad Prism (v10.2.1). RStudio (v2023.03.0).

For manuscripts utilizing custom algorithms or software that are central to the research but not yet described in published literature, software must be made available to editors and reviewers. We strongly encourage code deposition in a community repository (e.g. GitHub). See the Nature Portfolio guidelines for submitting code & software for further information.

Data

Policy information about availability of data

All manuscripts must include a data availability statement. This statement should provide the following information, where applicable:

- Accession codes, unique identifiers, or web links for publicly available datasets
- A description of any restrictions on data availability
- For clinical datasets or third party data, please ensure that the statement adheres to our policy

All data supporting the findings of this study are available within the paper and its Supplementary Information.

Research involving human participants, their data, or biological material

Policy information about studies with human participants or human data. See also policy information about sex, gender (identity/presentation), and sexual orientation and race, ethnicity and racism.

Reporting on sex and gender	The term sex is used as representing a biological attribute. The sex of each brain donor is reported in the paper and was determined based on self-reported biological sex assigned at birth. Consent has been obtained for sharing of individual-level data and the donors are anonymized. A sex-based analysis has been performed for the determination of sex-matched groups. Information on gender (shaped by social and cultural circumstances) has not been collected.
Reporting on race, ethnicity, or other socially relevant groupings	The brain donors included in our study were recruited by the Netherlands Brain Bank. Their ethnicity is not recorded in the clinical files. However, all participants are of Dutch nationality. Ethnicity data is not collected for this study.
Population characteristics	The brain donors were sex- and age-matched and did not receive disease-modifying therapies.
Recruitment	The participants were recruited by the Netherlands Brain Bank through a brain donor program. The donors included in our study were selected based on the presence of grey matter in the brain tissue blocks.
Ethics oversight	Vrij University, The Netherlands; The Netherlands Brain Bank; NINDS USA (protocol # NCT00001248) and the University of Toronto, Canada (protocol #30813)

Note that full information on the approval of the study protocol must also be provided in the manuscript.

Field-specific reporting

Please select the one below that is the best fit for your research. If you are not sure, read the appropriate sections before making your selection.

☒ Life sciences ☐ Behavioural & social sciences ☐ Ecological, evolutionary & environmental sciences

For a reference copy of the document with all sections, see nature.com/documents/nr-reporting-summary-flat.pdf

Life sciences study design

All studies must disclose on these points even when the disclosure is negative.

Sample size	We performed a power analysis using G*Power based on data from previous experiments. Specifically, the effect size of BTK treatment on TLT and subpial pathology ranges from 1.4 for the presence of B220+ cells, 2.1 for CD3+ cells, and >6 for quantification of PLP staining. Based on alpha error probability of 0.05 and power of 0.8, minimum n=4 each of treated vs. control mice will be needed to observe statistical significance in a two-tailed Mann-Whitney test for an effective size of 2.1.
Data exclusions	No data were excluded from the analyses.
Replication	Each experiment was repeated 2 or 3 times.
Randomization	Experimental groups were randomly assigned.
Blinding	Investigators were blinded to group allocation during data collection and analysis.

Reporting for specific materials, systems and methods

We require information from authors about some types of materials, experimental systems and methods used in many studies. Here, indicate whether each material, system or method listed is relevant to your study. If you are not sure if a list item applies to your research, read the appropriate section before selecting a response.

Materials & experimental systems

n/a	Involved in the study
☐	☒ Antibodies
☒	☐ Eukaryotic cell lines
☒	☐ Palaeontology and archaeology
☐	☒ Animals and other organisms
☐	☒ Clinical data
☒	☐ Dual use research of concern
☒	☐ Plants

Methods

n/a	Involved in the study
☒	☐ ChIP-seq
☐	☒ Flow cytometry
☐	☒ MRI-based neuroimaging

Antibodies

Antibodies used

For all antibodies used in this study: the target, the clone number, the source, the catalogue number and the dilution used are provided in supplementary table 2.

Mouse flow
CD3-PE mAb, 17A2 1:200 Biolegend, 100206
CD4-BV421 mAb, RM4-5 1:200 Biolegend, 100543
IL17a-PerCP Cy5.5 mAb, 17B7 1:100 eBioscience, 45-7177
INFγ-PE-Cy7 mAb, XMG1.2 1:200 eBioscience, 25-7311
GM-CSF- FITC mAb, MP1- 22E9 1:100 eBioscience, 11-7331
CD45-BUV395 30-F11 1:500 BD, 564279
CD19-BUV661 1D3 1:200 Invitrogen, 376-0193-82
CD4-BV421 RM4-5 1:200 Biolegend, 119507
B220-BV711 RA3-6B2 1:200 Biolegend, 103255
CD3-FITC 17A2 1:200 Biolegend, 100204
LTBR,FC Fusion HiP Recombinant LTBR (28-221-Fc(IgG1) 1:400 bps b71122
Goat anti-human IgG Fc Secondary Antibody-PE polyclonal 1:500 Invitrogen, 12-4998-82
Mouse IF
CD3-AF594 mAb, 17A2 1:100 Biolegend, 100240
B220-AF488 mAb, RA3- 6B2 1:100 Thermo scientific, 53-0452-82
BAFF mAb, Sandy-2 1:100 AdipoGen Life Sciences
Mouse IHC
PLP mAb, plpc1 1:100a Bio-Rad, MCA839G
Iba-1 mAb, EPR16589 1:8000a Abcam, ab92305
Neurofilament light chain mAb, 8A1 1:200a Santa Cruz Biotech, sc-20012
GFAP pAb 1:4000a Dako, Z0334
CXCL13 pAb 1:500b Biorbyt, orb318720
Human IHC
Proteolipid protein (PLP) mAb, plpc1 1:3000c Biorad, MCA839G
CD3 mAb, SP7 1:500 d Novus Biological, NB600-1441
CD20 mAb, L26 1:1000a Abcam, ab9475
CD68 mAb, PGM1 1:200a Dako,
Human leukocyte antigen (HLA)-DR mAb, LN3 8.6µg/mld Biolegend, 327002

Validation

All antibodies were titrated and negative controls (omission of secondary antibody or isotype controls) were used in each staining run.

Animals and other research organisms

Policy information about studies involving animals; ARRIVE guidelines recommended for reporting animal research, and Sex and Gender in Research

Laboratory animals

Female 6- to 10-week-old (young) and 8 to 12-months-old (old) SJL/J mice, and LTb-/- mice were used in this study.

Wild animals

The study did not involve wild animals.

Reporting on sex

In this study we only used female mice. We have performed experiments in male mice and found similar outcomes. However, experimental autoimmune encephalomyelitis in male mice is associated with health and behavioural complications. Therefore, we decided to continue the study in females only.

Field-collected samples

The study did not involve samples collected in the field.

Ethics oversight

The university of Toronto approved and provided guidance on the study protocol (#20011363).

Note that full information on the approval of the study protocol must also be provided in the manuscript.

Clinical data

Policy information about clinical studies

All manuscripts should comply with the ICMJE guidelines for publication of clinical research and a completed CONSORT checklist must be included with all submissions.

Clinical trial registration

Provide the trial registration number from ClinicalTrials.gov or an equivalent agency.

Study protocol

Note where the full trial protocol can be accessed OR if not available, explain why.

Data collection

Describe the settings and locales of data collection, noting the time periods of recruitment and data collection.

Outcomes

Describe how you pre-defined primary and secondary outcome measures and how you assessed these measures.

Plants

Seed stocks — *Report on the source of all seed stocks or other plant material used. If applicable, state the seed stock centre and catalogue number. If plant specimens were collected from the field, describe the collection location, date and sampling procedures.*

Novel plant genotypes — *Describe the methods by which all novel plant genotypes were produced. This includes those generated by transgenic approaches, gene editing, chemical/radiation-based mutagenesis and hybridization. For transgenic lines, describe the transformation method, the number of independent lines analyzed and the generation upon which experiments were performed. For gene-edited lines, describe the editor used, the endogenous sequence targeted for editing, the targeting guide RNA sequence (if applicable) and how the editor was applied.*

Authentication — *Describe any authentication procedures for each seed stock used or novel genotype generated. Describe any experiments used to assess the effect of a mutation and, where applicable, how potential secondary effects (e.g. second site T-DNA insertions, mosiacism, off-target gene editing) were examined.*

Flow Cytometry

Plots

Confirm that:

☒ The axis labels state the marker and fluorochrome used (e.g. CD4-FITC).

☒ The axis scales are clearly visible. Include numbers along axes only for bottom left plot of group (a 'group' is an analysis of identical markers).

☒ All plots are contour plots with outliers or pseudocolor plots.

☒ A numerical value for number of cells or percentage (with statistics) is provided.

Methodology

Sample preparation

Leptomeninges were removed from the brainstem, cerebellum, ventricles, hypothalamus, and cortex into digestion buffer (10 mM HEPES, 150 mM NaCl, 1 mM MgCl2, 5 mM KCl, and 1.8 mM CaCl2 in HBSS buffer) containing DNAse I (60 µg/mL) and collagenase D (1 mg/mL). Collected cells from leptomeninges were washed twice in ice-cold PBS and resuspended in complete RPMI (10% FBS from Gibco, Thermo Fisher Scientific; l-glutamine from MilliporeSigma, sodium pyruvate from MilliporeSigma, penicillin from MilliporeSigma, streptomycin from MilliporeSigma, HEPES pH 7.0 from Gibco, Thermo Fisher Scientific; and β-mercaptoethanol from Gibco, Thermo Fisher Scientific, in RPMI-1640 medium from MilliporeSigma). Cells were counted with a hemocytometer and incubated at 37°C for 5 hours with an intracellular cytokine restimulation buffer (PMA [MilliporeSigma, stock 500 µg/mL] used at 1:100,000; ionomycin [MilliporeSigma, stock 0.5 mg/mL] used at 1:1000; and Brefeldin A [eBioscience, Thermo Fisher Scientific, stock 100x] used at 1:1000 in complete RPMI). At the end of the incubation, cells were collected, washed twice in ice-cold PBS, and resuspended in PBS with 2% FBS and stained with LIVE/DEAD Fixable Aqua (Life Technologies, Thermo Fisher Scientific) at 1:1000 in PBS for 30 minutes at 4°C, followed by staining with anti–CD4- (mAb, RM4-5), and anti–CD3- (mAb, 17A2) in PBS with 2% FBS and 1 mg/mL Fc block. Cells were then permeabilized with CytoFix/CytoPerm (BD Biosciences) for 20 minutes at 4°C, then stained with anti–GM-CSF-FITC (mAb, MP1- 22E9), anti–IL-17A-(mAb, 17B7), and anti–IFN-γ- (mAb, XMG1.2) in 1× Perm/Wash buffer with 1 mg/mL Fc block.

Spleens were collected and mashed through 70-µm filters into culture medium [RPMI 1640 (Sigma-Aldrich) supplemented with 10% fetal bovine serum (Gibco), 1× penicillin-streptomycin (Sigma-Aldrich), 1× L-Glutamin (Sigma-Aldrich)]. Splenocytes were resuspended in 5mL of RBC lysis buffer (Ebioscience 00-4333-57) for 5 min to remove red blood cells. Cells were washed and resuspended in culture media at 2x106/mL. 200ul of cell suspension /well were plated in 96-well U bottom culture plates. Cells were placed in the incubator at 37°C 5%CO2 for 1 hour to rest, then BTK inhibitor (or culture medium) was added at a concentration of 10nM for 1 hour. InVivoMAb anti-mouse CD40 (BioxCell BE0016-2) (5ug/ml) + LPS (Sigma-Aldrich L2880) (1ug/ml) were added to the culture overnight (18-20 hours). Cells were harvested, washed with PBS and stained with Live/Dead Fixable Aqua (Invitrogen) at a dilution of 1:1000 for 20 min on ice. Surface markers were stained in 2% fetal bovine serum in PBS for 30 min on ice.

Instrument — BD LSR X-20 II instrument and FACSymphony A3

Software — FACSDiva software (BD Biosciences) for acquisition. FlowJo V10.5.3 software for analysis.

Cell population abundance — We did not perform cell sorting. Not applicable

Gating strategy — Lymphocyte gate (starting cell population) was determined according to the SSC and FSC. Next we gated on Single cells using FSC-H and FSC-A then SSC-H and SSC-A. On the single cells, we gated on the Aqua negative population to select live cells. Using Fluorescence Minus One (FMO)s for CD3, CD4, IFN-γ, IL-17A and GM-CSF, we set the axes and the gates and determined where our negative and positive populations are. On live cells, for T cells we gated on the CD3+ CD4+ cell population and then determined the % of positive cells for IFN-γ, IL-17A and GM-CSF within the CD3+ CD4+ cell. For B cells we gated on the CD45+ CD19+ B220+ cells, and we determined the % of B220+ LTb+ cells.

☒ Tick this box to confirm that a figure exemplifying the gating strategy is provided in the Supplementary Information.

Magnetic resonance imaging

Experimental design

Design type	Post-mortem MRI of mouse brains
Design specifications	4 to 8 brains per group were scanned using A 7-Tesla 306 mm horizontal-bore magnet (BioSpec 70/30 USR, Bruker) with a ParaVision 6.0.1 console
Behavioral performance measures	MRI data from naive mice and EAE mice either treated with BTKi or vehicle alone were compared. Results are expressed as mean volume normalized by the axial lenght of the brain skull + or - SD.

Acquisition

Imaging type(s)	Structural MRI
Field strength	7 Tesla
Sequence & imaging parameters	T2W 3D FSE cylindrical k-space acquisition sequence, TR/TE/ETL = 350 ms/12 ms/6, TEeff = 30 ms, 4 effective averages, FOV/matrix size = 20.2 × 20.2 × 25.2 mm/504 × 504 × 630, total imaging time = 13.2 hours.
Area of acquisition	whole brain scan

Diffusion MRI ☐ Used ☒ Not used

Preprocessing

Preprocessing software	All anatomical brain images were registered together using the mni autoreg and Advanced Normalizations Tools tool kits. The resulting consensus average and Jacobian determinants were used to quantifying volumetric differences between each MRI image and the average. The MAGeT pipeline was used to segment images using a published classified MRI.
Normalization	Results were normalized by the axial length of the brain skull
Normalization template	All anatomical brain images were registered together using the mni autoreg and Advanced Normalizations Tools tool kits.
Noise and artifact removal	not applicable
Volume censoring	not applicable

Statistical modeling & inference

Model type and settings	*Specify type (mass univariate, multivariate, RSA, predictive, etc.) and describe essential details of the model at the first and second levels (e.g. fixed, random or mixed effects; drift or auto-correlation).*
Effect(s) tested	Data were analyzed using Kruskal-Wallis test with correction for multiple comparisons.

Specify type of analysis: ☒ Whole brain ☐ ROI-based ☐ Both

Statistic type for inference (See Eklund et al. 2016)	The anatomical images had an isotropic resolution of 40 µm voxels.
Correction	not applicable

Models & analysis

n/a	Involved in the study
☒	☐ Functional and/or effective connectivity
☐	☒ Graph analysis
☒	☐ Multivariate modeling or predictive analysis

Graph analysis	Data were analyzed using Kruskal-Wallis test with correction for multiple comparisons.